Cascade Drug-Release Strategy for Enhanced Anticancer Therapy

Xu Zhang[1], **Sheng Wang**[1,*], **Guohui Cheng**[1], **Peng Yu**[1], **Jin Chang**[1,*], **Xiaoyuan Chen**[2,*]

[1]School of Life Sciences, Tianjin University and Tianjin Engineering Center of Micro-Nano Biomaterials and Detection-Treatment Technology, Tianjin 300072, China

[2]Yong Loo Lin School of Medicine and Faculty of Engineering, National University of Singapore, Singapore, 117597, Singapore

SUMMARY

Chemotherapy serves as one of the most effective approaches in numerous tumor treatments but also suffers from the limitations of low bioavailability and adverse side effects due to premature drug leakage. Therefore, it is crucial to realize accurate on-demand drug release for promoting the application of chemotherapeutic agents. To achieve this, stimuli-responsive nanomedicines that can be activated by delicately designed cascade reactions have been developed in recent years. In general, the nanomedicines are triggered by an internal or external stimulus, generating an intermediate stimulus at tumor site, which can intensify the differences between tumor and normal tissues; the drug release process is then further activated by the intermediate stimulus. In this review, the latest progress made in cascade reactions-driven drug-release modes, based on the intermediate stimuli of heat, hypoxia, and reactive oxygen species, is systematically summarized. The perspectives and challenges of cascade strategy for drug delivery are also discussed.

INTRODUCTION

Chemotherapy, a common method in the treatment of a variety of tumors, has been extensively used in the clinic.[1,2] However, compared with local treatments such as surgical operation and radiotherapy, chemotherapy is a systemic therapy approach whereby the administered chemotherapeutic agents are nonspecifically distributed in most of the tissues through blood circulation.[3] Considering that most traditional chemotherapeutic drugs cannot distinguish cancer cells and normal cells, the non-targeted drug distribution,[4,5] which causes unsatisfactory efficacy and severe side effects, is deemed to be one of the major factors that restrict chemotherapy.[6,7] Therefore, the successful delivery of drugs to specific sites of action by overcoming many physicochemical, biopharmaceutical, and pharmacokinetic barriers is essential.[8] Although the development of nanocarriers offers a new avenue to realize targeted drug delivery by utilizing the enhanced permeability and retention effect,[9] many issues, such as premature drug leakage and nonspecific interactions with the tumor

microenvironment (TME), still need to be addressed.[10] The ideal nanomedicines are expected to maintain stable structures in normal tissue and blood circulation while releasing chemotherapeutic agents specifically at the tumor site.[11]

For the purpose of achieving precise controlled drug release, stimuli-responsive drug-delivery nanoplatforms whose release behavior can be activated or accelerated by endogenous or exogenous stimuli at the tumor site have been developed.[12–16] The endogenous stimuli mainly include typical TME states, such as pH, redox status, and specific enzymes, while common exogenous stimuli include light, heat, and ultrasound.[17,18] Unfortunately, drug release triggered by endogenous stimuli is usually confronted with the problem of low selectivity. For example, many designs of stimuli-responsive nanomedicines are based on the mildly acidic condition of tumor (~pH 6.8), which is different from that of the bloodstream and normal tissues (~pH 7.4).[19] However, the pH of human body fluids is under dynamic equilibrium and some organelles are acidic both in tumor cells and normal cells, such as endosome and lysosome.[20] On the other hand, although exogenous stimuli offer high selectivity to tumor tissue, the low responsiveness becomes an obstacle in exogenous stimuli-responsive nanomedicines. For instance, most of the photoresponsive moieties, such as azobenzene and *o*-nitrobenzyl groups, usually need to be activated by UV or visible light with high laser power density, leading to limited *in vivo* biomedical application effects.[21–23]

To develop stimuli-responsive drug-release systems with high selectivity and rapid response for enhanced anticancer therapy, a cascade strategy has been employed in many designs of nanomedicines in recent years.[24,25] Cascade reactions are also known as domino-type reactions, which enable multistep reactions to be triggered step by step through careful design in a sequence. In cascade drug-release strategy, the nanomedicines are triggered by an internal or external stimulus, generating an intermediate stimulus at the tumor site, which can augment the differences between tumor and normal tissues. The drug-release process will then be further activated by the intermediate stimulus. Therefore, this strategy is a promising way to improve both selectivity and responsivity of nanomedicines by TME remodeling.[26] In addition, the cascade strategy is also promising for the design of a combination therapy system. For example, the combination of photothermal agents and thermal-responsive drug carriers can realize concurrent photothermal therapy (PTT) and controlled drug release.[27] Moreover, some tumor treatments, such as photodynamic therapy (PDT)[28] and chemodynamic therapy (CDT),[29] rely on the generation of reactive oxygen species (ROS) to damage cancer cells. Therefore, the combination of chemotherapy and ROS-based therapy offers the possibility for cascade reactions-driven drug release by using ROS-responsive nanocarriers.

Here, we summarize recent advances in cascade reactions-driven drug-release modes for tumor therapy. In these modes, the intermediate stimuli include heat, hypoxia, and ROS (Figure 1). Many different stimuli-responsive materials that can respond to the intermediate stimuli and achieve structural changes have been used for designs and developments of nanoplatforms (Table 1). In brief, the purpose of this review is not merely to concentrate on the mechanisms of controlled drug delivery and release behaviors in cascade reactions but

also to provide rational designs to meet new challenges and expand applications in future clinical tumor-targeted chemotherapy.

HEAT

The concept of stimuli-responsive drug delivery, first put forward in the late 1970s, applied local drug release using thermosensitive liposomes.[56] Since then many kinds of thermal-responsive materials, such as lower critical solution temperature (LCST) polymers and ammonium bicarbonate (ABC), have been applied in the design and development of drug-delivery systems.[57–61] In the past decades, various stimuli-triggered heat-generation approaches, such as photothermal, sonothermal, and microwave-thermal, have been studied for local thermogenesis.[62] The combination of these approaches and thermal-responsive materials thus represents a strategy for the design of cascade reactions-driven drug-release systems.[63] The advantage of this drug-release strategy is to achieve targeted drug release and precise therapy through external stimuli-responsive local thermal changes. In this strategy, the main drug-release modes include heat-induced linker cleavage, structural changes of drug carriers, radical generation, and multiple responses.

Heat-Induced Linker Cleavage

Thermal change usually results in many other changes of nanomedicines, such as heat-induced linker cleavage.[64] In this cascade-release mode, chemotherapeutic drugs are usually conjugated to nanocarriers via thermosensitive chemical bonds that can be endothermically broken to accomplish the drug release. For example, Hu's group developed light-controlled heat-producing pulsatile drug-release nanoparticles (denoted as CPT@DOX-UCST/PPy), which consisted of upper critical solution temperature (UCST) polymer conjugated with thermosensitive doxorubicin (DOX) prodrug, hydrophobic camptothecin (CPT) in the micellar core, and a polypyrrole (PPy) outer shell.[30] Upon 808-nm near-infrared (NIR) laser irradiation, the PPy shell can generate heat through a photothermal effect. The thermolabile azo bond cleavage and particle size swelling caused by heat further lead to DOX prodrug activation and release of encapsulated CPT (Figure 2A). This light-controlled dual drug-release system combined PTT with chemotherapy and avoided the leakage of drugs in blood circulation. As illustrated in Figure 2B, with the increased time of laser irradiation, temperature increased accordingly and the rate was directly proportional to the nanoparticle (NP) content and laser power density. In response to the temperature change, reversible NP swelling (~106 nm at 60°C) and shrinking (~70 nm at 25°C) was observed (Figure 2C). As expected, at 60°C, both DOX and CPT were continuously released with cumulative release rates of 68% and 75%, respectively. In contrast, negligible drug leakage was observed at 37°C (Figure 2D). These results suggested that the drug-release behaviors of both DOX and CPT were closely related to thermal changes. Because PPy is an efficient photothermal conversion material, the heat-induced linker cleavage can also be triggered by NIR laser irradiation. The release rates of dual drugs were obviously accelerated by light irradiation, while both significantly declined when the light was off (Figure 2E). The intracellular drug release of the CPT@DOX-UCST/PPy was verified by confocal laser scanning microscopy (CLSM) analysis. In the absence of NIR light irradiation, the DOX fluorescence was hardly detected inside cells due to the quenching effect of PPy, indicating minimal drug leakage

(Figure 2F). However, upon laser illumination, distinct DOX fluorescence was observed in the cell nucleus, indicating that the release of DOX could be driven by light-heat-linker cleavage cascade reactions.

Heat-Induced Structural Changes of Drug Carriers

The generation of heat can not only cleave linkers but also sometimes lead to the conformational change of drug carriers. Apart from the size expansion as mentioned above, other structural changes of nanocarriers, such as DNA strand separation,[65,66] changes of hydrophobicity,[33,34] shrinkage of thermoresponsive segments,[57] and destruction caused by bubble generation[35,67] can be triggered by hyperthermia.

Farokhzad's group used DNA assembly to construct a targeted and NIR-responsive drug-delivery nanoplatform (denoted as transfer DNA(DOX)-NRs).[31] The transfer DNA(DOX)-NRs were composed of cDNA strands, gold nanorods (NRs), and polyethylene glycol (PEG) layers. The chemotherapeutic drug, DOX, was loaded onto DNA strands through the sites provided by sequential -CG-base pairs. Under NIR light irradiation, gold NRs transformed light into heat and therefore triggered DOX release due to the heat-induced DNA double-helix denaturation.[68,69] Therefore, this strategy can realize selective release of drugs by light-induced thermal changes, achieving local thermo-chemotherapy of tumor.

Through the sequence design of DNA linker, its drug loading capacity and thermal denaturation can be controlled to modulate the drug-release rate. For example, Raeesi et al. proposed a core-satellite controllable drug-delivery modular nanosystem.[32] This system took gold nanorods (GNRs) as the ''core'' architecture and was decorated with gold NPs as ''satellites'' through DNA linkers (Figure 3A). Three sequences of DNA linkers were designed by adjusting sequence length and composition. After loading DOX in the middle loading zone, three core-satellite carriers (LDox1, LDox2, and LDox3) were obtained. Compared with LDox1, LDox2 and LDox3 showed higher DOX-loading efficiencies due to the increased linker sequence lengths. The DOX release triggered by the cascade of heat generation and DNA dehybridization was further studied. As shown in Figure 3B, upon laser irradiation, the drug-release rates of both LDox2 and LDox3 were increased along with laser exposure time. Compared with LDox2, LDox3 showed faster drug-release rate under the same condition. The complete drug-release time of LDox3 (4 min) was one-third that of LDox2 (12 min). Correspondingly, the drug-release onset temperature of LDox3 (~58°C) was lower than that of LDox2 (~68°C), which was due to the decreased melting temperature of DNA linkers in LDox3 (Figure 3C). The relatively low trigger temperature of LDox3 made it suitable for cascade reactions-driven drug release. In addition, this system can achieve ''additive'' therapeutic effects of PTT and triggered drug release.

Based on the photothermal effect of gold nanomaterials, Yavuz et al. also developed a nanoplatform using smart polymer coated gold nanocages (AuNGs).[33] The thermoresponsive copolymer with an LCST at 39°C, poly(N-isopropylacrylamide)-co-polyacrylamide (pNIPAAm-co-pAAm), was anchored to the surface of drug-loaded porous AuNGs. At body temperature (37°C), the pores on AuNGs were closed by hydrophilic pNIPAAm-co-pAAm polymer coating to prevent drug leakage. Upon NIR light irradiation, heat generated from photothermal effect leads to hydrophilic-to-hydrophobic transition of

the coated polymers, resulting in collapse of polymer chains and consequent exposure of the pores for drug release. Interestingly, this hydrophilic-to-hydrophobic transition of polymers is reversible. The polymer will return to the initial state and stop drug release when laser is turned off. Therefore, by manipulating laser irradiation, the release dosage can be controlled.

Liu et al. proposed another design of nanocarrier by exploiting heat-induced pore exposure. [34] Concretely, yolk-shell Fe_3O_4@Au NPs composed of small Fe_3O_4 cores and porous gold outer shells were prepared (Figure 3D) whereby the chemotherapeutic drug, DOX, could be loaded in the large space provided by the hollow cavity of the Fe_3O_4@Au NPs. The thermosensitive polymer (pNIPAm-co-pAAm) was used to endow the nanomedicine with stimuli-triggered drug-release properties. Upon NIR laser irradiation, the gold shell of Fe_3O_4@Au NPs absorbed light energy and converted it into heat, leading to increased surrounding temperature (Figure 3E). As a result, NIR light-triggered drug release was realized through polymer collapse and pore exposure (Figure 3F). The intracellular DOX release of yolk-shell Fe_3O_4@Au NPs was demonstrated by fluorescence distribution inside cells. After NIR laser irradiation, DOX signal was detected in both cytoplasm and nucleus, confirming NIR photothermally triggered drug release.

Nanocarrier destruction caused by bubble generation is another important direction in the design of cascade reactions-driven drug-release systems. For example, Sung's group proposed a liposomal system (abbreviated as AuNG-Lips) in which therapeutic drug AuNG and bubble-generating agent ABC were simultaneously loaded (Figure 3G). [35] As mentioned, AuNG is an efficient photothermal conversion agent that can absorb the energy of NIR light and convert it to localized heat. As shown in Figure 3H, the AuNG-Lips suspensions had a dose-dependent temperature rise upon NIR laser irradiation. ABC is a thermosensitive material that can be decomposed to produce CO_2, ammonia, and water when the local temperature is over $40°C$. [70] Therefore, the NIR irradiation-induced heating further led to CO_2 bubble generation inside liposomes (Figure 3I). As shown in Figure 3J, in the absence of NIR laser ($37°C$), a relatively small percentage of DOX was released from AuNG-Lips; however, under NIR irradiation ($42°C$), instantaneous DOX release was observed. As the transition temperature of liposomes was about $52°C$, [71] this release behavior was a result of internal CO_2 bubble-induced liposome destruction rather than the direct heating.

Heat-Induced Radical Generation

Cancer treatment approaches based on the generation of ROS or radicals are promising for enhancement of therapeutic efficacy on account of their overcoming the hypoxic microenvironment. [72,73] For example, Akkaya's group proposed a singlet oxygen ($^1O_2$) generation nanoplatform which was composed of anthracene endoperoxide derivative (EPT1) functionalized gold nanorods (AuNR) (Figure 4A). [36] EPT1 is a reliable chemical source of ROS. Upon heating, EPT1 was shown to generate $1O_2$ through heat-induced cycloreversion of endoperoxides. The NIR light-induced $1O_2$ generation of EPT1-AuNR was evaluated by using a $^1O_2$ probe, 1,3-diphenyliso-benzofuran (DPBF). Compared with AuNR without EPT1, the NIR light-irradiated EPT1-AuNR led to obvious decrease of DPBF absorbance (Figure 4B), indicating effective generation of $^1O_2$. The light-induced

ROS generation inside cells was evaluated by an ROS sensor. Under laser irradiation, the AuNR did not cause intracellular ROS generation; however, the EPT1-AuNR significantly improved the ROS level (Figure 4C). These results demonstrated that the light-induced $^1O_2$ generation was attributed to the photothermal heating of AuNR and subsequent decomposition–cycloreversion process of EPT1.

Moreover, a common initiator, 2,2′-azobis[2-(2-imidazolin-2-yl)propane] dihydrochloride (AIPH), which can be expeditiously decomposed to generate alkyl radicals under heat stimulation, provides a promising approach to solving the problem of tumor hypoxia and enhanced anticancer effect.[74,75] Shen et al. demonstrated a nanosystem (Au-PCM-AIPH) to generate free radicals for cancer therapy by using AuNGs loaded with a phase-change material (PCM) and AIPH, as shown in Figure 4D,[37] whereby PCM is melted under NIR irradiation via the photothermal effect of AuNGs, resulting in rapid release and decomposition of AIPH. By adjusting the power density and irradiation time of laser, the AIPH release behavior could be regulated (Figure 4E). The AIPH decomposition and free radical generation were measured by the determination of $ABTS^+$, which was produced by the reaction between 2,2′-azino-bis(3-ethylbenzothiazoline-6-sulfonic acid) (ABTS) and free radical. The generation efficiency of $ABTS^+$. at 44°C was obviously higher than that at 37°C (Figure 4F). This temperature-dependent generation of $ABTS^+$. indicated that the AIPH release and decomposition were faster at higher temperature. Since the radical is able to damage various cellular components, the generation of AIPH radical was further characterized by using red blood cells (RBCs) as models. One of the end products of lipid peroxidation, methane dicarboxylic aldehyde (MDA), was chosen as an indication of cell damage. As shown in Figure 4G, the MDA level was noticeably increased under NIR laser irradiation compared with that without laser irradiation. As shown in Figure 4H, under NIR light irradiation, AIPH-based free radicals were generated inside Au-PCM-AIPH-incubated cancer cells under both normoxic and hypoxic conditions, suggesting that the generation of free radical was not dependent on intracellular oxygen level. Furthermore, NIR light irradiation overtly enhanced the ability of Au-PCM-AIPH in suppressing cancer cells, confirming that the free radicals were generated through the cascade of photothermal effect and heat-induced AIPH decomposition (Figure 4I).

Regarding improvement of the photoinduced partial hyperthermia effect in cancer treatment, the second NIR window (NIR-II, 1,000–1,350 nm) has attracted much attention. Compared with the conventional NIR window (NIR-I, 650–950 nm), NIR-II light has deeper tissue penetration and higher maximum exposure permission.[76–78] Lin's group proposed a free-radical-generating nanosystem by using an NIR-II photothermal agent.[38] A $CuFeSe_2$ nanoparticle with high conversion efficiency was cladded with polydopamine for AIPH loading. After BSA modification, $CuFeSe_2$-AIPH@BSA with dual-peak absorption in both NIR-I and NIR-II regions was obtained for cascade reaction-induced generation of free radicals. The temperature of $CuFeSe_2$-AIPH@BSA was obviously increased upon NIR laser irradiation. Correspondingly, the release rates of AIPH and free radicals from the $CuFeSe_2$-AIPH@BSA increased with temperature increment. Moreover, NIR-II (1,064 nm) treatment showed higher therapeutic efficacy than NIR-I (808 nm).

Heat-Induced Multiple Responses

By combining different thermoresponsive materials, the design of heat-induced multiple responses has also been applied to develop drug-delivery systems. Tang et al. proposed a logic-gated system-based modular nanomedicine (v-ACED$_2$) to realize accurate on-demand drug release by exploiting heat-induced prodrug activation and carrier destruction.[39] As shown in Figure 5A, this system consisted of DOX prodrug, AIPH, and ROS-responsive amphiphilic polymer. Among them, hydrophobic DOX prodrug (denoted as CED$_2$) was fabricated by conjugation of two DOX molecules onto the photothermal organic dye (CR780) via Edman linkers.[79] The two different ''AND'' logical gates were formed by four associative units: mild hyperthermia (I, caused by photothermal agent), acidic pH (II, TME), free radicals (III, generated by heat-induced AIPH decomposition), and nanocarrier disintegration (IV). Upon NIR laser irradiation, the CR780 dye can effectively convert light energy to heat, resulting in obvious temperature increase (Figure 5C). The DOX prodrug can be activated by acidic pH and NIR laser-elevated temperature (AND1) due to the degradation of Edman linker in the CED$_2$ prodrug (Figures 5B and 5D). Meanwhile, AIPH was decomposed under laser-induced heating to generate free radicals, which further oxidized the ROS-responsive polymer, poly(-propylene sulfide)-poly(ethylene glycol) (PPS-PEG), and caused nanovesicle destruction (Figure 5E). Therefore, the DOX release can be controlled by prodrug activation and vesicle destruction (AND2). To verify the logic gates-controlled drug-release behavior of the v-A-CED$_2$, release profiles were measured in an acidic condition (pH 5.0) with NIR laser treatment (heated up to 42°C). As Figure 5F indicates, compared with v-A-CD$_2$ (without Edman linkers) and v-CED$_2$ (without AIPH), v-A-CED$_2$ showed the most efficient NIR-triggered DOX release, which confirmed that drug release was driven by heat-induced linker cleavage and nanovesicle destruction. Furthermore, the intracellular distribution of DOX in U87MG cells was observed by confocal microscopy (Figure 5G). For the v-A-CED$_2$ + L group, the fluorescence of free DOX was obviously accumulated in the nucleus, indicating logic-gated release under laser irradiation; while for the other control vesicles DOX fluorescence was concentrated in cytosol, suggesting little to no DOX release. The cascade reactions-driven logic-gated release mode can reduce toxicity in normal tissues.

HYPOXIA

Hypoxia caused by insufficient supply of oxygen and nutrient is a typical feature of the solid TME.[80] By taking advantage of oxygen-level difference between normal tissues and tumor tissue, hypoxia-targeted drug delivery has been considered as a promising way to achieve specific chemotherapy.[26] Meanwhile, many tumor treatment approaches also need to consume oxygen in the process. For example, PDT is an oxygen-dependent approach by converting oxygen into toxic ROS, such as $^1O_2$.[17] In addition, glucose oxidase (GOD) can transform oxygen to hydrogen peroxide (H_2O_2) and cut off nutritional supply in tumor-starvation therapy.[44] These oxygen-consuming processes lead to exacerbation of TME hypoxia state and provide a new avenue for the design of cascade reactions-driven drug release. The main modes of hypoxia-responsive drug release include linker cleavage, hydrophobic-to-hydrophilic transition, activation of prodrug, and multiple responses.

Hypoxia-Induced Linker Cleavage

The design of nanocarriers containing hypoxia-responsive linker is a typical method to achieve hypoxia-triggered drug release. For example, the azobenzene (AZO) group (−N=N−) is a hypoxia-sensitive linker that can be cleaved by reductases under hypoxic condition.[81] Based on this linker, Liu's group proposed a nanocarrier composed of AZO groups containing conjugated polymers (CPs) for co-encapsulation of photosensitizer (Ce6) and anticancer drug (CPT).[40] The obtained CPs-CPT-Ce6 NPs can achieve triggered drug release through light-enhanced hypoxia response. As displayed in Figure 6A, upon laser irradiation oxygen consumption occurred in the Ce6-mediated PDT process, intensifying tumor hypoxia condition. The hypoxia-induced activation of azoreductase would then lead to the cleavage of hypoxia-sensitive AZO linkers, resulting in promoted dissociation of CPs. Therefore, the hypoxic condition induced by PDT could be used as an intermediate stimulus for triggering CPT release. Fluorescence imaging was carried out to confirm PDT-induced intracellular oxygen consumption by using a hypoxia probe. As shown in Figure 6B, when HeLa cells were treated with photosensitizer-containing NPs (CPs-Ce6 NPs) and laser irradiation, red fluorescence of the hypoxia probe was observed inside cells; this result was similar to that for the positive control group, hypoxia inducer (deferoxamine, DFO)-treated cells. In contrast, in the groups without Ce6 or laser irradiation, cells did not show fluorescence, indicating that the intracellular hypoxic condition was induced by PDT process in which photosensitizer and light were essential. Moreover, hypoxia-triggered degradation of AZO groups containing CPs and subsequent activation of CPT release were demonstrated by intracellular drug distribution (Figure 6C). In the presence of light irradiation, the intensity of intracellular CPT fluorescence was significantly stronger than that without light irradiation, indicating that CPT release was triggered by light-mediated cascade reactions. The cancer cell-killing efficiencies of different groups under light irradiation were evaluated. The CPs-CPT NPs group without photosensitizer showed negligible anticancer effect because only a small amount of drug was released under normoxic conditions (Figure 6D). However, the Ce6-containing groups showed obvious anticancer effects due to PDT. The cell-killing effect of CPs-Ce6-CPT NPs was significantly enhanced when compared with that of CPs-Ce6 NPs, indicating the combination effect of PDT and hypoxia-induced drug release.

Hypoxia-sensitive linkers can also be used to conjugate drug molecules and polymers for the preparation of hypoxia-responsive polyprodrugs. Cui et al. reported a polyprodrug nanomedicine (SPNpd) based on a light-responsive amphiphilic semiconducting polymer (SP).[41] A chemotherapeutic drug that can induce DNA crosslinking and cellular apoptosis, bromoisophosphoramide mustard intermediate (IPM-Br), was conjugated to the semiconducting polymer through hypoxia-cleavable linker (Figure 6E). The SPNpd was then prepared through self-assembly of amphiphilic SP. Drug-free nanoparticles (SPNc) were also prepared as a control group. Under 808-nm light irradiation, the SP in SPNpd could be used as a photosensitizer for tumor oxygen consumption and $^1O_2$ generation, leading to exacerbation of tumor hypoxia. Catalyzed by nitroreductase (NTR), the nitro groups in SPNpd were reduced by intracellular nicotinamide adenine dinucleotide (NADH) in a hypoxic environment, allowing activation of drug release. As shown in Figure 6F, upon incubation with NTR and NADH under hypoxic condition for 6 h, an elution peak

representing IPM-Br was found in the high-performance liquid chromatography (HPLC) profile of SPNpd, indicating hypoxia-triggered linker cleavage and free drug release. The synergistic therapy effect of SPNpd was further evaluated on 4T1 cancer cells. Whether or not laser irradiation was applied, SPNpd and SPNc showed similar cytotoxicities under normoxic conditions (Figure 6G), indicating that little or no drug was released. However, in the hypoxic environment, the viability of SPNpd-treated cells was lower than that of the SPNc-treated group regardless of whether NIR light irradiation was applied (Figure 6H). These results confirmed that the drug release of SPNpd activated by hypoxia can amplify the cancer therapeutic effect through synergy with PDT.

Hypoxia-Induced Hydrophobic-to-Hydrophilic Transition

Apart from linker cleavage, the hypoxia-induced bioreduction of functional groups can also result in other structural changes of nanomedicines. The designs of such hypoxia-responsive nanomedicines usually require units with specific properties. For example, through an NTR-catalyzed single-electron bioreduction under hypoxic conditions, hydrophobic 2-nitroimidazole (NI) can be converted to hydrophilic 2-aminoimidazoles (AI).[82] Gu's group took good advantage of this feature of NI. They proposed an NI-grafted conjugated polymer (CP-NI)-based nanocarrier for chemotherapeutic drug (DOX) encapsulation, obtaining a hypoxia-responsive nanoformulation (denoted as DOX/CP-NI NPs).[42] The dithiophene-benzotriazole moiety in CP can be used as a photosensitizer to consume oxygen and produce $^1O_2$ upon light irradiation, leading to local hypoxia (Figure 7A). Due to the NI-to-AI transition triggered by hypoxia, the hydrophobic polymer CP-NI would become hydrophilic, leading to disassembly of nanocarrier. Therefore, the encapsulated drugs were released in a cascade action. As indicated in Figure 7B, the drug release from DOX/CP-NI NPs was significantly accelerated by laser illumination at both pH 7.4 and 5.4, demonstrating that the drug-release behavior was directly correlated with the bioreduction of NI groups rather than acid-base condition. Moreover, under several laser on-off cycles, drugs were released almost exclusively upon light irradiation (Figure 7C), which further confirmed that the release of drugs was controlled by the cascade of light-triggered oxygen consumption and hypoxia-activated nanocarrier dissociation. CLSM was used to investigate the light-induced cellular hypoxia and intracellular release of DOX. The fluorescence of hypoxia detection probe was observed inside HeLa cells with incubation of CP-NI NPs and light irradiation, indicating a hypoxic intracellular environment caused by the PDT process. The DOX fluorescence was mainly distributed in endosome/lysosome of HeLa cells incubated with DOX/CP-NI NPs. However, upon light irradiation, free DOX was released and accumulated in the nuclei, demonstrating the enhancement of drug release triggered by light-induced hypoxia (Figure 7D). In terms of therapy effect, the tumor growth was entirely suppressed by administration of DOX/CP-NI NPs under light irradiation, which further validated the light-induced hypoxia-activated cascade drug release in tumor therapy.

Hypoxia-Induced Activation of Prodrug

The design of prodrugs is a promising approach for reducing side effects *in vivo* because prodrugs need to be activated to exert a pharmacological effect.[83] In past decades, various hypoxia-activated prodrugs, such as quinone-based prodrugs and N-oxide prodrugs, have been developed for selective treatment of cancer.[84] In some oxygen-consuming therapies,

the oxygen consumption-induced tumor local hypoxia can be simultaneously used as a trigger to activate hypoxia-selective prodrug. By combining PDT and hypoxia-selective prodrug, Feng et al. designed a liposome-based nanoplatform (AQ4N-hCe6-liposome) through co-loading of hypoxia-activated prodrug (AQ4N) and photosensitizer (hexadecylamine conjugated chlorin e6, hCe6) (Figure 8A).[43] AQ4N is an alkyl N-oxide prodrug that can be activated in reducing environment to produce AQ4, an effective DNA intercalator/topoisomerase poison, leading to ca. 100-fold higher toxicity.[85] Upon laser irradiation, the tumor local hypoxic environment caused by the hCe6-mediated PDT process led to the conversion of prodrug from AQ4N to AQ4. Therefore, the AQ4N-hCe6-liposome showed hypoxia-dependent cytotoxicity to cancer cells. As a result, the antitumor activity of AQ4N-hCe6-liposome with light irradiation was obviously higher than that without light irradiation, attributed to the cascade of PDT and hypoxia-activated chemotherapy.

GOD-related therapy is another oxygen-consuming approach because GOD can convert glucose into hydrogen peroxide and gluconic acid through a catalytic reaction whereby oxygen is used as an electron acceptor. Yang et al. reported a cascaded drug-delivery system based on stepwise degradable yolk-shell dendritic mesoporous organo-silica nanoparticle (YS-DMONs).[44] As shown in Figure 8B, GOD and AQ4N were loaded into the large-pore dendritic shell and the small-pore yolk, respectively. Owing to high intracellular glutathione (GSH) level, the fast disintegration of the shell led to rapid release of GOD and AQ4N (process i). The released GOD then induced starvation, H_2O_2 production, and local hypoxia through oxidation of glucose (process ii). Hypoxia further activated the prodrug AQ4N to AQ4 (process iii). The YS-DMONs-AQ4N-GOD possessed potent ability for suppressing tumor growth, indicating that the cascade delivery of GOD and AQ4N is a promising strategy for tumor inhibition.

Besides AQ4N, another commonly used hypoxia-selective prodrug is tirapazamine (TPZ), which can be stimulated to generate toxic radicals in hypoxic environment through enzymatic reduction.[86] Zhang et al. reported a TPZ and GOD co-loaded amorphous calcium carbonate ($CaCO_3$) nanoparticle for synergistic tumor-starvation therapy and chemotherapy. [45] As shown in Figure 8C, in acidic intratumoral environment, the decomposition of $CaCO_3$ led to accelerated release of GOD and TPZ. The exacerbated hypoxia caused by GOD-driven oxidation reaction further activated TPZ to produce toxic radicals through a single-electron reduction reaction. The activated TPZ radicals were then further used to induce cell apoptosis.

Hypoxia-Induced Multiple Responses

By combining two or more hypoxia-responsive units, nanosystems with the property of hypoxia-induced multiple responses were proposed. Gu's group presented an anaerobe nanovesicle mimic (designated as TPZ/AI-NV) by combining hypoxia-responsive polymer and hypoxia activatable prodrug TPZ (Figure 9A).[46] The nanovesicles were assembled by light-harvesting Ce6-modified polymer and NI-grafted amphiphilic polymer. The prodrug, TPZ, was loaded into the aqueous core of nanovesicles (Figure 9B). The light-triggered photochemical reaction of Ce6 led to rapid oxygen consumption and ROS generation and the corresponding hypoxia accelerated the hydrophobic-to-hydrophilic transition of NI-

grafted polymer, leading to dissociation of nanovesicles and release of TPZ. In the meantime, the released TPZ molecules were activated to benzotriazinyl radicals through a bioreduction reaction. As shown in Figure 9C, triggered by light irradiation, obvious dissociation and size decrease of TPZ/AI-NV were observed, leading to accelerated release of TPZ. As shown in Figure 9D, after 10 min of laser irradiation, a burst release of TPZ was observed within 6 h. In contrast, TPZ was released from TPZ/AI-NV at a very slow rate in the dark. Moreover, the AI-NV-mediated ROS generation and intracellular hypoxic condition under light irradiation were verified by using CLSM. Non-irradiated cells incubated with AI-NV did not show fluorescence. However, upon light irradiation, obvious fluorescence of ROS and hypoxia were observed in AI-NV-incubated cells, indicating light-triggered oxygen consumption and ROS generation. The cargo TPZ had a selective cytotoxicity to hypoxic tumor cells but hardly influenced the normal cells.[87] Therefore, the free TPZ, AI-NV, and TPZ/AI-NV without light irradiation showed negligible cytotoxicities toward HepG2 cells due to inefficient ROS generation and TPZ activation (Figure 9E). Light irradiation did not affect the cytotoxicity of free TPZ due to the absence of oxygen-consuming photosensitizer (Figure 9F). However, upon light irradiation, the cytotoxicity of TPZ/AI-NV was obviously higher than that of AI-NV, which further confirmed the synergy of light-induced PDT and hypoxia-activated chemotherapy.

ROS

A variety of tumor therapeutic modalities, such as CDT,[88–93] PDT,[94–96] radiotherapy,[97] thermodynamic therapy,[98] and sonodynamic therapy (SDT),[99] can produce ROS for cancer cell killing. For example, PDT, the most widely used approach for ROS generation, is a process that involves the photosensitizer-mediated conversion from oxygen into $^1O_2$ under light irradiation; while CDT involves generation of highly oxidative hydroxyl radicals through the Fenton and Fenton-like reactions. Over the past decades, various ROS-responsive materials have been developed; therefore, the cascade of ROS generation and ROS-triggered drug release can be a promising approach to achieve targeted drug delivery, especially in combination therapy. The common approaches to ROS-responsive drug-release modes include ROS-induced linker cleavage, hydrophobic-to-hydrophilic transition, and multiple responses.

ROS-Induced Linker Cleavage

Various ROS-sensitive linkers, such as thioketal (TK) linker,[100–102] peroxalate ester linker, [103,104] and boronic ester linker,[105] have been applied in the design of ROS-responsive drug-delivery nanosystems. Typically, ROS-sensitive linkers are designed in the chemical structures of nanocarriers and prodrugs.

The development of ROS-responsive nanocarriers is the commonly used approach to realize ROS-controlled drug release. Yang's group explored a polymeric nanocarrier (TK-PPE@NP), which was assembled by ROS-sensitive poly(thioketal phosphoester) (TK-PPE) for ROS-triggered drug release (Figure 10A).[47] The chemotherapeutic drug (DOX) and photosensitizer (Ce6) were encapsulated into the hydrophobic core of the TK-PPE@NP. Under laser irradiation, ROS generated through the Ce6-mediated PDT process would cause

the cleavage of TK linkers and decomposition of TK-PPE *in situ*, leading to the shrinkage of TK-PPE@NP$_{Ce6/DOX}$ and the consequent burst release of loaded DOX. The design of prodrugs is another strategy to overcome high systemic toxicity of free drugs.[106–109] For example, Phua et al. proposed supramolecular NPs (HA-aPS-aCPT NPs) formed by β-cyclodextrin (CD) conjugated hyaluronic acid (HA), adamantane-conjugated photosensitizer THPP (aPS), and adamantane-TK linker-CPT prodrug (aCPT).[48] Because of the inclusion complex formed by CD and adamantane, stable supramolecular NPs could be obtained through self-assembly. Light irradiation would lead to activation of aCPT prodrug and release of free CPT drug via ROS-triggered thioketal linker cleavage. Therefore, HA-aPS-aCPT NPs could realize light-controlled combination therapy of PDT and chemotherapy. The TK linker was also used to develop prodrugs to realize cascade activation of puromycin aminonucleoside and immune checkpoint inhibitor (NLG919).[49,50] In another study, Pu's group reported an organic semiconducting pro-nanoenzyme (OSPE) for cascade reactions-driven therapeutic enzyme release.[51] As shown in Figure 10B, the OSPE was prepared by conjugating phenylboronic acid pinacol group-caged ribonuclease A (EBAP) to semiconducting polymer nanoparticle (SPN) through a $^1O_2$-cleavable linker, (*Z*)-2,2′-(ethene-1,2-diyl-bis(sulfanediyl))diethanamine (BSDA). Upon NIR laser irradiation, the $^1O_2$ generated from SPN-mediated PDT process would cause rapid release of EBAP due to cleavage of linker. The EBAP would be further activated by endogenous H_2O_2 to induce the degradation of RNA, resulting in cell death.

ROS produced by chemical processes can also be used to trigger drug release. For example, with the help of nanoscale metal organic framework (MOF) carriers, Cheng et al. developed a biomimetic cascade nanoreactor (Mem@GOD@ZIF-8@BDOX).[10] GOD was encapsulated in ZIF-8 MOF for intracellular glucose consumption to realize starvation therapy; meanwhile, the generated H_2O_2 further triggered release and activation of H_2O_2-sensitive doxorubicin prodrug (BDOX). Therefore, this nanoreactor could be used for tumor-targeted starvation therapy and activated chemotherapy. In addition, Ge's group reported a pH/ROS dual-responsive GOD-loaded nanoreactor (GOD@PCPT-NR) constructed from ROS-responsive polyprodrug polymersome, in which GOD was encapsulated in the inner aqueous cavity (Figure 10C).[52,110] In blood circulation and normal tissues, the GOD@PCPT-NR remained inactive due to tight encapsulation of GOD; however, in the acidic TME, the increased membrane permeability of polymersome allowed glucose and O_2 to diffuse into the nanoreactor. The activation of oxidation reaction led to generation of H_2O_2, which further triggered drug release from polyprodrug via linker cleavage. Therefore, this nanoreactor can achieve combination of oxidation therapy and chemotherapy.

In the past few years, some novel therapeutic agents that can tumor-specifically generate ROS, such as β-lapachone (Lapa), have attracted great attention. Lapa can increase the intracellular H_2O_2 level via the catalysis of the reduced nicotinamide adenine dinucleotide (phosphate) (NAD(P)H): quinone oxidoreductase-1 (NQO1) enzyme, which serves as a specific biomarker in various kinds of cancer cells.[111] For example, Rao's group developed a cascade amplification release nanoparticle (CARN) by encapsulating Lapa and a H_2O_2-activatable prodrug (BDOX) in polymeric micelle.[105] The BDOX prodrug was derived from DOX by incorporating a boronate moiety. In tumor cells, the released Lapa would increase the H_2O_2 level, leading to activation of BDOX through boronic ester linker cleavage. Due to

the low NQO1 expression in normal cells, the CARN could realize minimal side effects by avoiding undesired prodrug activation. Furthermore, the futile redox cycles of Lapa consumed NAD(P)H and adenosine triphosphate (ATP), leading to downregulation of P-glycoprotein expression; therefore, CARN could overcome multidrug resistance of cancer cells. Chen's group also developed a Lapa-loaded dual-responsive nanomedicine (PtkDOX-NM) that was assembled by pH-responsive polymer and ROS-activatable PEG-block-polythioketal prodrug (PEG-PtkDOX).[53] As shown in Figure 10D, in cancer cells Lapa was rapidly released due to the intracellular acidic environment-triggered disassembly of PtkDOX-NMs, resulting in increased H_2O_2 level. In the presence of chelated iron, H_2O_2 was converted to hydroxyl radicals through Fenton reaction and further triggered cascade release of DOX via ROS-responsive thioketal linker cleavage. The PtkDOX-NMs were able to effectively suppress tumor growth *in vivo*, which proved the effects of ROS-triggered cascade drug release in synergistic chemo- and chemodynamic therapy.

ROS-Induced Hydrophobic-to-Hydrophilic Transition

The ROS-triggered hydrophilicity changes of the polymers can also lead to the collapse of the polymeric drug nanocarriers and controlled release of drugs. Under oxidative conditions, the hydrophobic sulfur-, selenium-, and tellurium-containing polymers can undergo hydrophobic-to-hydrophilic transition.[112] Based on this phenomenon, Zhou et al. proposed a DOX-loaded nanovesicle (denoted as Au-LAHP-vDOX) formed by ROS-responsive PPS-PEG and linoleic acid hydroperoxide (LAHP)-modified Au NPs for X-ray-triggered drug release and synchronous chemoradiation.[54] In general, high-energy X-rays can be applied in radiotherapy to promote intracellular ROS level. X-ray-activated ROS generation can potently overcome the light-penetration depth restriction of the conventional visible light-triggered PDT. In this study, upon X-ray irradiation, hydroxyl radicals were generated from the X-ray labile LAHP molecules, leading to *in situ* oxidation of PPS (Figure 11A). The hydrophobic PPS became hydrophilic due to the oxidation of thioether, resulting in the disassembly of nanovesicles and rapid drug release. As shown in the drug-release profiles (Figure 11B), negligible DOX release was observed in the groups without LAHP or X-ray irradiation. However, upon X-ray irradiation, a burst drug release was observed in the Au-LAHP-vDOX group. Transmission electron microscopy (TEM) images further confirmed the swelling and structural contraction of Au-LAHP-vDOX triggered by X-ray irradiation or external H_2O_2 (Figures 11C and 11D). To investigate the intracellular production of ROS and drug distribution, U87MG cells with different treatments were detected by using CLSM analysis. An ROS indicator, 2,7-dichlorodihydro fluorescein diacetate (DCFH-DA), was chosen for intracellular ROS imaging. The cells treated with Au-LAHP-vDOX and X-ray irradiation exhibited the highest intracellular ROS level due to the X-ray-induced generation of hydroxyl radicals (Figure 11E). Noticeably, DOX showed different intracellular distributions according to the magnified images. Under X-ray irradiation, the DOX fluorescence was mainly distributed in cytosols of Au-LA-vDOX (without LAHP)-treated U87MG cells; however, DOX was obviously accumulated in the nuclei of cells treated with Au-LAHP-vDOX, indicating the cascade reactions-driven drug release. Owing to the X-ray-triggered free radical generation and subsequent drug release, the Au-LAHP-vDOX showed the most potent cytotoxicity (Figure 11F). Furthermore, the simultaneous drug release

during radiotherapy may significantly mitigate the possible emergence of resistance to monotherapy, thereby enhancing the synergistic effect of chemoradiotherapy.[113]

ROS-Induced Multiple Responses

By combining the ROS-sensitive prodrug and ROS-induced structural change of nanocarrier, Zhou et al. proposed a ROS-activatable DOX prodrug vesicle (RADV) by anchoring the prodrug and photosensitizer in liposomal bilayer membrane through self-assembly.[55] As shown in Figure 12A, the RADV was composed of unsaturated 1,2-dioleoyl-*sn*-glycero-3-phosphocholine (DOPC), TK linker-based DOX prodrug (PPC-TK-Dox), PEG-modified pyropheophorbide-a (PPa-PEG), and cholesterol. RADV can induce localized ROS generation at the tumor site upon laser irradiation, leading to cleavage of TK linker and oxidation of the unsaturated DOPC (Figure 12B). Under the combination effect of ROS-induced prodrug activation and increased lipid membrane permeability, DOX can be rapidly released from the RADV upon light irradiation. In this manner, RADV allows local-regional chemotherapy and PDT in a spatiotemporally controlled way. liquid chromatography-mass spectrometry was applied to confirm the laser-induced activation of prodrug. As shown in Figure 12C, almost all the PPC-TK-Dox prodrug was activated within 5 min of irradiation. As shown in Figure 12D, about 78% of activated drug was released from RADV under 5 min of light irradiation. In contrast, less than 20% of drug was released from ROS-inactivatable DOX prodrug vesicle (RIADV) under the same conditions, indicating that the drug release was triggered by ROS-induced TK linker cleavage. To further elucidate the ROS-induced multiple responses, saturated phospholipid (DSPC) was used to replace unsaturated DOPC for the preparation of RADV and RIADV. The drug-release rate of DSPC-incorporated RADV was 1.8-fold lower than that of original RADV prepared by DOPC (Figure 12E), suggesting that the structural change of nanovesicles caused by DOPC oxidation was also an important factor for light-triggered rapid drug release. CLSM was carried out to investigate the intracellular ROS generation and drug distribution. In RADV-treated cells, DOX (red fluorescence) was entrapped in the lysosomal vesicles surrounding the cell nucleus without irradiation (Figure 12F). However, upon laser irradiation, ROS (green fluorescence) was generated and further triggered prodrug activation. The activated drugs were released into cytosol and subsequently transferred to the nuclei. Prodrug activation was quenched if vitamin C was added as an ROS scavenger, indicating cascade reactions-driven drug release. In contrast, RIADV was unable to be activated by laser irradiation due to ROS-insensitive conjugation. These results demonstrated that ROS-activatable prodrug and permeability change of nanocarriers play a synergistic positive effect on drug-release behaviors. The antitumor effect of RADV was further evaluated by cytotoxicity assay. Laser irradiation significantly decreased the viability of cells treated with RADV, which was attributed to ROS generation and drug release. However, in the presence of vitamin C, the antitumor effect of RADV was dramatically inhibited because both ROS generation and prodrug activation were quenched.

CONCLUSION AND OUTLOOK

To improve anticancer efficacy, ideal nanomedicines ought to preferentially accumulate in tumor tissue, complete cellular internalization immediately, and target the release of

effective components. However, the full chemotherapeutic benefit is always limited by the nonspecific biodistribution of drugs, which leads to systemic cytotoxicity and low success rate of drug delivery to the tumor sites. To address this issue, many novel stimuli-responsive drug-release nanoplatforms based on a cascade strategy have been developed over the last few years. The intermediate stimuli of novel nanomedicines after initial stimuli can aggravate the differences between normal and tumor tissues, which are served as the switch-triggered drug release. To some extent, the cascade drug-release strategy can control on-demand drug release and avoid the nontargeting leakage, which has great potential to enhance the efficacy and reduce side effects.

This review systematically summarized three kinds of typical cascade drug-release modes. Although some progress continues to be made at present, some issues still need to be addressed in the future. For example, various cascade reactions are triggered by light, whose tissue penetration depth was limited. In addition, the scope of thermal changes may restrict the relevant drug-release rate and the possibility of clinical application. Many tumor treatments require participation of oxygen, such as dynamic-related therapy, which restricts the applications of drug release triggered by hypoxic conditions. In addition, some ROS that can trigger drug release, such as hydroxyl radical, are unfortunately able to influence even damaged normal cells. Therefore, further research about cascade strategy is needed to realize the targeted drug release for enhanced anticancer therapy.

To provide promising approaches of precision chemotherapy and expand the clinical application in the future, the following aspects should be taken into consideration:

1. Selectivity. Chemotherapy is a systemic treatment, so it is essential to ensure that the targeted release of drug is mainly at the tumor site to minimize the side effects. In the cascade drug-release strategy, the intermediate stimuli of novel nanomedicines after initial stimuli should be able to expand the differences between normal and tumor tissues to ensure accurate drug release. The development of NIR-II light-activated cascade reactions may be a promising way to achieve both high selectivity and deep tissue penetration because of reduced light scattering and minimized tissue absorption of NIR-II light.

2. Sensitivity. Ideally, chemotherapeutic agents should be released timely once reaching the tumor site, so the sensitivity of the triggering mechanism in the complex designs of cascade reactions must be ensured to reduce the loss and delay period of drug efficacy.

3. Efficiency. The designs of nanomedicines should take the triggering mechanism of drug release into full consideration, especially in combination therapy, for example when hypoxia-induced drug-release mode used in combination with treatments that require oxygen may limit the therapeutic effects of each other. In ROS-induced drug-release mode, ROS will be seriously consumed during the drug-release process; therefore, it is difficult to achieve a satisfactory combination treatment outcome.

4. Clinical trials. Most of the aforementioned studies were carried out under extreme conditions that are not relevant to pathophysiology, so the practical use

of drug-release modes triggered by cascade reactions in chemotherapy are still in the early development phase due to the lack of clinical evidence. More systematic evaluations are still urgently required to achieve clinical transformation in tumor chemotherapy.

We hope that this review is timely for summarizing the current status about cascade drug-release strategy and will contribute to the development and application of drug-delivery nanoplatforms for tumor-targeted chemotherapy.

ACKNOWLEDGMENTS

REFERENCES

1. Yoo J-W, Irvine DJ, Discher DE, and Mitragotri S (2011). Bio-inspired, bioengineered and biomimetic drug delivery carriers. Nat. Rev. Drug Discov 10, 521–535. [PubMed: 21720407]

2. Jain RK, and Stylianopoulos T (2010). Delivering nanomedicine to solid tumors. Nat. Rev. Clin. Oncol 7, 653–664. [PubMed: 20838415]

3. Chen D, Tang Y, Zhu J, Zhang J, Song X, Wang W, Shao J, Huang W, Chen P, and Dong X (2019). Photothermal-pH-hypoxia responsive multifunctional nanoplatform for cancer photo-chemo therapy with negligible skin phototoxicity. Biomaterials 221, 119422. [PubMed: 31437723]

4. Cheng Z, Al Zaki A, Hui JZ, Muzykantov VR, and Tsourkas A (2012). Multifunctional nanoparticles: cost versus benefit of adding targeting and imaging capabilities. Science 338, 903–910. [PubMed: 23161990]

5. Thakor AS, and Gambhir SS (2013). Nanooncology: the future of cancer diagnosis and therapy. Ca-cancer J. Clin 63, 395–418. [PubMed: 24114523]

6. Dai Y, Xu C, Sun X, and Chen X (2017). Nanoparticle design strategies for enhanced anticancer therapy by exploiting the tumour microenvironment. Chem. Soc. Rev 46, 3830–3852. [PubMed: 28516983]

7. Ren Z, Sun S, Sun R, Cui G, Hong L, Rao B, Li A, Yu Z, Kan Q, and Mao Z (2020). A metal-polyphenol-coordinated nanomedicine for synergistic cascade cancer chemotherapy and chemodynamic therapy. Adv. Mater 32, 1906024.

8. Cheetham AG, Chakroun RW, Ma W, and Cui H (2017). Self-assembling prodrugs. Chem. Soc. Rev 46, 6638–6663. [PubMed: 29019492]

9. Bjornmalm M, Thurecht KJ, Michael M, Scott AM, and Caruso F (2017). Bridging bio-nano science and cancer nanomedicine. ACS Nano 11, 9594–9613. [PubMed: 28926225]

10. Cheng H, Jiang X-Y, Zheng R-R, Zuo S-J, Zhao L-P, Fan G-L, Xie B-R, Yu X-Y, Li S-Y, and Zhang X-Z (2019). A biomimetic cascade nanoreactor for tumor targeted starvation therapy-amplified chemotherapy. Biomaterials 195, 75–85. [PubMed: 30616030]

11. Wang S, Huang P, and Chen X (2016). Hierarchical targeting strategy for enhanced tumor tissue accumulation/retention and cellular internalization. Adv. Mater 28, 7340–7364. [PubMed: 27255214]

12. He X, Chen X, Liu L, Zhang Y, Lu Y, Zhang Y, Chen Q, Ruan C, Guo Q, Li C, et al. (2018). Sequentially triggered nanoparticles with tumor penetration and intelligent drug release for pancreatic cancer therapy. Adv. Sci 5, 1701070.

13. Mura S, Nicolas J, and Couvreur P (2013). Stimuli-responsive nanocarriers for drug delivery. Nat. Mater 12, 991–1003. [PubMed: 24150417]

14. He X, Zhang J, Li C, Zhang Y, Lu Y, Zhang Y, Liu L, Ruan C, Chen Q, Chen X, et al. (2018). Enhanced bioreduction-responsive diselenide-based dimeric prodrug nanoparticles for triple negative breast cancer therapy. Theranostics 8, 4884–4897. [PubMed: 30429875]

15. Li J, and Pu K (2020). Semiconducting polymer nanomaterials as near-infrared photoactivatable protherapeutics for cancer. Acc. Chem. Res 53, 752–762. [PubMed: 32027481]

16. Zhang Y, Xu C, Yang X, and Pu K (2020). Photoactivatable protherapeutic nanomedicine for cancer. Adv. Mater 32, 2002661.

17. Zhou Z, Song J, Nie L, and Chen X (2016). Reactive oxygen species generating systems meeting challenges of photodynamic cancer therapy. Chem. Soc. Rev 45, 6597–6626. [PubMed: 27722328]

18. Mai BT, Fernandes S, Balakrishnan PB, and Pellegrino T (2018). Nanosystems based on magnetic nanoparticles and thermo- or pH-responsive polymers: an update and future perspectives. Acc. Chem. Res 51, 999–1013. [PubMed: 29733199]

19. Karimi M, Ghasemi A, Sahandi Zangabad P, Rahighi R, Moosavi Basri SM, Mirshekari H, Amiri M, Shafaei Pishabad Z, Aslani A, Bozorgomid M, et al. (2016). Smart micro/nanoparticles in stimulus-responsive drug/gene delivery systems. Chem. Soc. Rev 45, 1457–1501. [PubMed: 26776487]

20. Ge Z, and Liu S (2013). Functional block copolymer assemblies responsive to tumor and intracellular microenvironments for site-specific drug delivery and enhanced imaging performance. Chem. Soc. Rev 42, 7289–7325. [PubMed: 23549663]

21. Lucky SS, Soo KC, and Zhang Y (2015). Nanoparticles in photodynamic therapy. Chem. Rev 115, 1990–2042. [PubMed: 25602130]

22. Yan B, Boyer J-C, Branda NR, and Zhao Y (2011). Near-infrared light-triggered dissociation of block copolymer micelles using upconverting nanoparticles. J. Am. Chem. Soc 133, 19714–19717. [PubMed: 22082025]

23. Deng H, Lin L, Wang S, Yu G, Zhou Z, Liu Y, Niu G, Song J, and Chen X (2019). X-ray-controlled bilayer permeability of bionic nanocapsules stabilized by nucleobase pairing interactions for pulsatile drug delivery. Adv. Mater 31, 1903443.

24. Davoodi P, Lee LY, Xu Q, Sunil V, Sun Y, Soh S, and Wang C-H (2018). Drug delivery systems for programmed and on-demand release. Adv. Drug Deliv. Rev 132, 104–138. [PubMed: 30415656]

25. Wang W, Liang G, Zhang W, Xing D, and Hu X (2018). Cascade-promoted photo-chemotherapy against resistant cancers by enzyme-responsive polyprodrug nanoplatforms. Chem. Mater 30, 3486–3498.

26. Yin W, Ke W, Chen W, Xi L, Zhou Q, Mukerabigwi JF, and Ge Z (2019). Integrated block copolymer prodrug nanoparticles for combination of tumor oxidative stress amplification and ROS-responsive drug release. Biomaterials 195, 63–74. [PubMed: 30612064]

27. He Y, Cong C, Li X, Zhu R, Li A, Zhao S, Li X, Cheng X, Yang M, and Gao D (2019). Nano-drug system based on hierarchical drug release for deep localized/systematic cascade tumor therapy stimulating antitumor immune responses. Theranostics 9, 2897–2909. [PubMed: 31244931]

28. Li S-Y, Cheng H, Xie B-R, Qiu W-X, Zeng J-Y, Li C-X, Wan S-S, Zhang L, Liu W-L, and Zhang X-Z (2017). Cancer cell membrane camouflaged cascade bioreactor for cancer targeted starvation and photodynamic therapy. ACS Nano 11, 7006–7018. [PubMed: 28665106]

29. Wang S, Wang Z, Yu G, Zhou Z, Jacobson O, Liu Y, Ma Y, Zhang F, Chen ZY, and Chen X (2019). Tumor-specific drug release and reactive oxygen species generation for cancer chemo/chemodynamic combination therapy. Adv. Sci 6, 1801986.

30. Yang J, Zhai S, Qin H, Yan H, Xing D, and Hu X (2018). NIR-controlled morphology transformation and pulsatile drug delivery based on multifunctional phototheranostic nanoparticles for photoacoustic imaging-guided photothermal-chemotherapy. Biomaterials 176, 1–12. [PubMed: 29842986]

31. Xiao Z, Ji C, Shi J, Pridgen EM, Frieder J, Wu J, and Farokhzad OC (2012). DNA self-assembly of targeted near-infrared-responsive gold nanoparticles for cancer thermo-chemotherapy. Angew. Chem. Int. Ed 51, 11853–11857.

32. Raeesi V, Chou LYT, and Chan WCW (2016). Tuning the drug loading and release of DNA-assembled gold-nanorod superstructures. Adv. Mater 28, 8511–8518. [PubMed: 27501857]

33. Yavuz MS, Cheng Y, Chen J, Cobley CM, Zhang Q, Rycenga M, Xie J, Kim C, Song KH, Schwartz AG, et al. (2009). Gold nanocages covered by smart polymers for controlled release with near-infrared light. Nat. Mater 8, 935–939. [PubMed: 19881498]

34. Lin LS, Yang XY, Zhou ZJ, Yang Z, Jacobson O, Liu YJ, Yang A, Niu G, Song JB, Yang HH, et al. (2017). Yolk-shell nanostructure: an ideal architecture to achieve harmonious integration of magnetic-plasmonic hybrid theranostic platform. Adv. Mater 29, 1606681.

35. Chuang E-Y, Lin C-C, Chen K-J, Wan D-H, Lin K-J, Ho Y-C, Lin PY, and Sung H-W (2016). A FRET-guided, NIR-responsive bubble-generating liposomal system for in vivo targeted therapy with spatially and temporally precise controlled release. Biomaterials 93, 48–59. [PubMed: 27070992]

36. Kolemen S, Ozdemir T, Lee D, Kim GM, Karatas T, Yoon J, and Akkaya EU (2016). Remote-controlled release of singlet oxygen by the plasmonic heating of endoperoxide-modified gold nanorods: towards a paradigm change in photodynamic therapy. Angew. Chem. Int. Ed 55, 3606–3610.

37. Shen S, Zhu C, Huo D, Yang M, Xue J, and Xia Y (2017). A hybrid nanomaterial for the controlled generation of free radicals and oxidative destruction of hypoxic cancer cells. Angew. Chem. Int. Ed 56, 8801–8804.

38. Yang J, Xie R, Feng L, Liu B, Lv R, Li C, Gai S, He F, Yang P, and Lin J (2019). Hyperthermia and controllable free radical coenhanced synergistic therapy in hypoxia enabled by near-infrared-II light irradiation. ACS Nano 13, 13144–13160. [PubMed: 31609581]

39. Tang L, Yang Z, Zhou Z, Ma Y, Kiesewetter DO, Wang Z, Fan W, Zhu S, Zhang M, Tian R, et al. (2019). A logic-gated modular nanovesicle enables programmable drug release for on-demand chemotherapy. Theranostics 9, 1358–1368. [PubMed: 30867836]

40. Zhang X, Wu M, Li J, Lan S, Zeng Y, Liu X, and Liu J (2018). Light-enhanced hypoxia-response of conjugated polymer nanocarrier for successive synergistic photodynamic and chemo-therapy. ACS Appl. Mater. Interfaces 10, 21909–21919. [PubMed: 29882654]

41. Cui D, Huang J, Zhen X, Li J, Jiang Y, and Pu K (2019). A semiconducting polymer nano-prodrug for hypoxia-activated photodynamic cancer therapy. Angew. Chem. Int. Ed 58, 5920–5924.

42. Qian C, Yu J, Chen Y, Hu Q, Xiao X, Sun W, Wang C, Feng P, Shen Q-D, and Gu Z (2016). Light-activated hypoxia-responsive nanocarriers for enhanced anticancer therapy. Adv. Mater 28, 3313–3320. [PubMed: 26948067]

43. Feng L, Cheng L, Dong Z, Tao D, Barnhart TE, Cai W, Chen M, and Liu Z (2017). Theranostic liposomes with hypoxiaactivated prodrug to effectively destruct hypoxic tumors post-photodynamic therapy. ACS Nano 11, 927–937. [PubMed: 28027442]

44. Yang Y, Lu Y, Abbaraju PL, Azimi I, Lei C, Tang J, Jambhrunkar M, Fu J, Zhang M, Liu Y, et al. (2018). Stepwise degradable nanocarriers enabled cascade delivery for synergistic cancer therapy. Adv. Funct. Mater 28, 1800706.

45. Zhang M-K, Li C-X, Wang S-B, Liu T, Song X-L, Yang X-Q, Feng J, and Zhang X-Z (2018). Tumor starvation induced spatiotemporal control over chemotherapy for synergistic therapy. Small 14, 1803602.

46. Qian C, Feng P, Yu J, Chen Y, Hu Q, Sun W, Xiao X, Hu X, Bellotti A, Shen QD, et al. (2017). Anaerobe-inspired anticancer nanovesicles. Angew. Chem. Int. Ed 56, 2588–2593.

47. Cao Z, Ma Y, Sun C, Lu Z, Yao Z, Wang J, Li D, Yuan Y, and Yang X (2018). ROS-sensitive polymeric nanocarriers with red light-activated size shrinkage for remotely controlled drug release. Chem. Mater 30, 517–525.

48. Phua SZF, Xue C, Lim WQ, Yang G, Chen H, Zhang Y, Wijaya CF, Luo Z, and Zhao Y (2019). Light-responsive prodrug-based supramolecular nanosystems for site-specific combination therapy of cancer. Chem. Mater 31, 3349–3358.

49. Li J, Cui D, Huang J, He S, Yang Z, Zhang Y, Luo Y, and Pu K (2019). Organic semiconducting pro-nanostimulants for near-infrared photoactivatable cancer immunotherapy. Angew. Chem. Int. Ed 58, 12680–12687.

50. Li J, Cui D, Jiang Y, Huang J, Cheng P, and Pu K (2019). Near-infrared photoactivatable semiconducting polymer nanoblockaders for metastasis-inhibited combination cancer therapy. Adv. Mater 31, 1905091.

51. Li J, Huang J, Lyu Y, Huang J, Jiang Y, Xie C, and Pu K (2019). Photoactivatable organic semiconducting pro-nanoenzymes. J. Am. Chem. Soc 141, 4073–4079. [PubMed: 30741538]

52. Li J, Li Y, Wang Y, Ke W, Chen W, Wang W, and Ge Z (2017). Polymer prodrug-based nanoreactors activated by tumor acidity for orchestrated oxidation/chemotherapy. Nano Lett 17, 6983–6990. [PubMed: 28977746]

53. Wang S, Yu G, Wang Z, Jacobson O, Lin LS, Yang W, Deng H, He Z, Liu Y, Chen Z-Y, et al. (2019). Enhanced antitumor efficacy by a cascade of reactive oxygen species generation and drug release. Angew. Chem. Int. Ed 58, 14758–14763.

54. Zhou ZJ, Chan A, Wang ZT, Huang XL, Yu GC, Jacobson O, Wang S, Liu YJ, Shan LL, Dai YL, et al. (2018). Synchronous chemoradiation nanovesicles by X-ray triggered cascade of drug release. Angew. Chem. Int. Ed 57, 8463–8467.

55. Zhou F, Feng B, Wang T, Wang D, Cui Z, Wang S, Ding C, Zhang Z, Liu J, and Yu H (2017). Theranostic prodrug vesicles for reactive oxygen species-triggered ultrafast drug release and local-regional therapy of metastatic triple-negative breast cancer. Adv. Funct. Mater 27, 1703674.

56. Yatvin MB, Weinstein JN, Dennis WH, and Blumenthal R (1978). Design of liposomes for enhanced local release of drugs by hyperthermia. Science 202, 1290–1293. [PubMed: 364652]

57. Guo X, Li D, Yang G, Shi CL, Tang ZM, Wang J, and Zhou SB (2014). Thermo-triggered drug release from actively targeting polymer micelles. ACS Appl. Mater. Interfaces 6, 8549–8559. [PubMed: 24804870]

58. Lin YJ, Huang CC, Wan WL, Chiang CH, Chang Y, and Sung HW (2017). Recent advances in CO2 bubble-generating carrier systems for localized controlled release. Biomaterials 133, 154–164. [PubMed: 28437626]

59. Chu KF, and Dupuy DE (2014). Thermal ablation of tumours: biological mechanisms and advances in therapy. Nat. Rev. Cancer 14, 199–208. [PubMed: 24561446]

60. Boissenot T, Bordat A, Larrat B, Varna M, Chacun H, Paci A, Poinsignon V, Fattal E, and Tsapis N (2017). Ultrasound-induced mild hyperthermia improves the anticancer efficacy of both Taxol® and paclitaxel-loaded nanocapsules. J. Control Release 264, 219–227. [PubMed: 28867377]

61. Wu Q, Yu J, Li M, Tan LF, Ren XL, Fu CH, Chen ZZ, Cao F, Ren J, Li LF, et al. (2018). Nanoengineering of nanorattles for tumor treatment by ct imaging-guided simultaneous enhanced microwave thermal therapy and managing inflammation. Biomaterials 179, 122–133. [PubMed: 29981949]

62. Nam J, Son S, Ochyl LJ, Kuai R, Schwendeman A, and Moon JJ (2018). Chemo-photothermal therapy combination elicits anti-tumor immunity against advanced metastatic cancer. Nat. Commun 9, 1074. [PubMed: 29540781]

63. Wang ZY, Ju YM, Ali Z, Yin H, Sheng FG, Lin J, Wang BD, and Hou YL (2019). Near-infrared light and tumor microenvironment dual responsive size-switchable nanocapsules for multimodal tumor theranostics. Nat. Commun 10, 4418. [PubMed: 31562357]

64. Kang HM, Hu S, Cho MH, Hong SH, Choi Y, and Choi HS (2018). Theranostic nanosystems for targeted cancer therapy. Nano Today 23, 59–72. [PubMed: 31186672]

65. Shanmugam V, Chien YH, Cheng YS, Liu TY, Huang CC, Su CH, Chen YS, Kumar U, Hsu HF, and Yeh CS (2014). Oligonucleotides-assembled Au nanorod-assisted cancer photothermal ablation and combination chemotherapy with targeted dual-drug delivery of doxorubicin and cisplatin prodrug. ACS Appl. Mater. Interfaces 6, 4382–4393. [PubMed: 24559392]

66. Liang S, Xie ZX, Wei Y, Cheng ZY, Han YQ, and Lin J (2018). DNA decorated Cu9S5 nanoparticles as NIR light responsive drug carriers for tumor chemo-phototherapy. Dalton Trans 47, 7916–7924. [PubMed: 29790525]

67. Huang CC, Liao ZX, Lu HM, Pan WY, Wan WL, Chen CC, and Sung HW (2016). Cellular organelle-dependent cytotoxicity of iron oxide nanoparticles and its implications for cancer diagnosis and treatment: a mechanistic investigation. Chem. Mater 28, 9017–9025.

68. Huschka R, Zuloaga J, Knight MW, Brown LV, Nordlander P, and Halas NJ (2011). Light-induced release of DNA from gold nanoparticles: nanoshells and nanorods. J. Am. Chem. Soc 133, 12247–12255. [PubMed: 21736347]

69. Wijaya A, Schaffer SB, Pallares IG, and Hamad-Schifferli K (2009). Selective release of multiple DNA oligonucleotides from gold nanorods. ACS Nano 3, 80–86. [PubMed: 19206252]

70. Boddien A, Gartner F, Federsel C, Sponholz P, Mellmann D, Jackstell R, Junge H, and Beller M (2011). CO2- "neutral" hydrogen storage based on bicarbonates and formates. Angew. Chem. Int. Ed 50, 6411–6414.

71. Chen K-J, Liang H-F, Chen H-L, Wang Y, Cheng P-Y, Liu H-L, Xia Y, and Sung H-W (2013). A thermoresponsive bubble-generating liposomal system for triggering localized extracellular drug delivery. ACS Nano 7, 438–446. [PubMed: 23240550]

72. Xia R, Zheng X, Hu X, Liu S, and Xie Z (2019). Photothermal-controlled generation of alkyl radical from organic nanoparticles for tumor treatment. ACS Appl. Mater. Inter 11, 5782–5790.

73. Wang M, Zhao Y, Chang M, Ding B, Deng X, Cui S, Hou Z, and Lin J (2019). Azo initiator loaded black mesoporous titania with multiple optical energy conversion for synergetic photo-thermal-dynamic therapy. ACS Appl. Mater. Interfaces 11, 47730–47738. [PubMed: 31790193]

74. Wan Y, Lu G, Zhang J, Wang Z, Li X, Chen R, Cui X, Huang Z, Xiao Y, Chelora J, et al. (2019). A biocompatible free radical nanogenerator with real-time monitoring capability for high performance sequential hypoxic tumor therapy. Adv. Funct. Mater 29, 1903436.

75. Lei Q, Qiu W-X, Hu J-J, Cao P-X, Zhu C-H, Cheng H, and Zhang X-Z (2016). Multifunctional mesoporous silica nanoparticles with thermal-responsive gatekeeper for NIR light-triggered chemo/photothermal-therapy. Small 12, 4286–4298. [PubMed: 27376247]

76. Jiang Y, Zhao X, Huang J, Li J, Upputuri PK, Sun H, Han X, Pramanik M, Miao Y, Duan H, et al. (2020). Transformable hybrid semiconducting polymer nanozyme for second near-infrared photothermal ferrotherapy. Nat. Commun 11, 1857. [PubMed: 32312987]

77. Jiang Y, Upputuri PK, Xie C, Zeng Z, Sharma A, Zhen X, Li J, Huang J, Pramanik M, and Pu K (2019). Metabolizable semiconducting polymer nanoparticles for second near-infrared photoacoustic imaging. Adv. Mater 31, 1808166.

78. Tian R, Zeng Q, Zhu S, Lau J, Chandra S, Ertsey R, Hettie KS, Teraphongphom T, Hu Z, Niu G, et al. (2019). Albumin-chaperoned cyanine dye yields superbright NIR-II fluorophore with enhanced pharmacokinetics. Sci. Adv 5, eaaw0672. [PubMed: 31548981]

79. Tang L, Zhang F, Yu F, Sun W, Song M, Chen X, Zhang X, and Sun X (2017). Croconaine nanoparticles with enhanced tumor accumulation for multimodality cancer theranostics. Biomaterials 129, 28–36. [PubMed: 28324863]

80. Tang Q, Cheng Z, Yang N, Li Q, Wang P, Chen D, Wang W, Song X, and Dong X (2019). Hydrangea-structured tumor microenvironment responsive degradable nanoplatform for hypoxic tumor multimodal imaging and therapy. Biomaterials 205, 1–10. [PubMed: 30889497]

81. Kiyose K, Hanaoka K, Oushiki D, Nakamura T, Kajimura M, Suematsu M, Nishimatsu H, Yamane T, Terai T, Hirata Y, et al. (2010). Hypoxia-sensitive fluorescent probes for in vivo real-time fluorescence imaging of acute ischemia. J. Am. Chem. Soc 132, 15846–15848. [PubMed: 20979363]

82. He H, Zhu R, Sun W, Cai K, Chen Y, and Yin L (2018). Selective cancer treatment via photodynamic sensitization of hypoxia-responsive drug delivery. Nanoscale 10, 2856–2865. [PubMed: 29364314]

83. He ZM, Dai YL, Li XL, Guo D, Liu YJ, Huang XL, Jiang JJ, Wang S, Zhu GZ, Zhang FW, et al. (2019). Hybrid nanomedicine fabricated from photosensitizer-terminated metal-organic framework nanoparticles for photodynamic therapy and hypoxia-activated cascade chemotherapy. Small 15, 1804131.

84. Sharma A, Arambula JF, Koo S, Kumar R, Singh H, Sessler JL, and Kim JS (2019). Hypoxia-targeted drug delivery. Chem. Soc. Rev 48, 771–813. [PubMed: 30575832]

85. Brown JM, and William WR (2004). Exploiting tumour hypoxia in cancer treatment. Nat. Rev. Cancer 4, 437–447. [PubMed: 15170446]

86. Denny WA, and Wilson WR (2000). Tirapazamine: a bioreductive anticancer drug that exploits tumour hypoxia. Expert Opin. Invest. Drugs 9, 2889–2901.

87. Liu Y, Liu Y, Bu W, Cheng C, Zuo C, Xiao Q, Sun Y, Ni D, Zhang C, Liu J, et al. (2015). Hypoxia induced by upconversion-based photodynamic therapy: towards highly effective synergistic bioreductive therapy in tumors. Angew. Chem. Int. Ed 54, 8105–8109.

88. Tang Z, Liu Y, He M, and Bu W (2019). Chemodynamic therapy: tumour microenvironment-mediated Fenton and Fenton-like reaction. Angew. Chem. Int. Ed 58, 946–956.

89. Ranji-Burachaloo H, Gurr PA, Dunstan DE, and Qiao GG (2018). Cancer treatment through nanoparticle-facilitated Fenton reaction. ACS Nano 12, 11819–11837. [PubMed: 30457834]

90. Lin L-S, Huang T, Song J, Ou X-Y, Wang Z, Deng H, Tian R, Liu Y, Wang J-F, Liu Y, et al. (2019). Synthesis of copper peroxide nanodots for H2O2 self-supplying chemodynamic therapy. J. Am. Chem. Soc 141, 9937–9945. [PubMed: 31199131]

91. Lin LS, Song J, Song L, Ke K, Liu Y, Zhou Z, Shen Z, Li J, Yang Z, Tang W, et al. (2018). Simultaneous fenton-like ion delivery and glutathione depletion by MnO2-based nanoagent to enhance chemodynamic therapy. Angew. Chem. Int. Ed 57, 4902–4906.

92. Zhou Z, Song J, Tian R, Yang Z, Yu G, Lin L, Zhang G, Fan W, Zhang F, Niu G, et al. (2017). Activatable singlet oxygen generation from lipid hydroperoxide nanoparticles for cancer therapy. Angew. Chem. Int. Ed 56, 6492–6496.

93. Lin L, Wang S, Deng H, Yang W, Rao L, Tian R, Liu Y, Yu G, Zhou Z, Song J, et al. (2020). Endogenous labile iron pool-mediated free radical generation for cancer chemodynamic therapy. J. Am. Chem. Soc 142, 15320–15330. [PubMed: 32820914]

94. Ma Y, Li X, Li A, Yang P, Zhang C, and Tang B (2017). H2S-activable MOF nanoparticle photosensitizer for effective photodynamic therapy against cancer with controllable singlet-oxygen release. Angew. Chem. Int. Ed 56, 13752–13756.

95. Yu G, Cen T-Y, He Z, Wang S-P, Wang Z, Ying X-W, Li S, Jacobson O, Wang S, Wang L, et al. (2019). Porphyrin nanocage-embedded single molecular nanoparticles for cancer nanotheranostics. Angew. Chem. Int. Ed 58, 8799–8803.

96. Yang W, Zhu G, Wang S, Yu G, Yang Z, Lin L, Zhou Z, Liu Y, Dai Y, Zhang F, et al. (2019). In situ dendritic cell vaccine for effective cancer immunotherapy. ACS Nano 13, 3083–3094. [PubMed: 30835435]

97. Zhang C, Zhao K, Bu W, Ni D, Liu Y, Feng J, and Shi J (2015). Marriage of scintillator and semiconductor for synchronous radiotherapy and deep photodynamic therapy with diminished oxygen dependence. Angew. Chem. Int. Ed 54, 1770–1774.

98. Xiang H, Lin H, Yu L, and Chen Y (2019). Hypoxia-irrelevant photonic thermodynamic cancer nanomedicine. ACS Nano 13, 2223–2235. [PubMed: 30624041]

99. Huang P, Qian X, Chen Y, Yu L, Lin H, Wane L, Zhu Y, and Shi J (2017). Metalloporphyrin-encapsulated biodegradable nanosystems for highly efficient magnetic resonance imaging-guided sonodynamic cancer therapy. J. Am. Chem. Soc 139, 1275–1284. [PubMed: 28024395]

100. Liu LH, Qiu WX, Li B, Zhang C, Sun LF, Wan SS, Rong L, and Zhang XZ (2016). A red light activatable multifunctional prodrug for image-guided photodynamic therapy and cascaded chemotherapy. Adv. Funct. Mater 26, 6257–6269.

101. Yuan Y, Liu J, and Liu B (2014). Conjugated-polyelectrolyte-based polyprodrug: targeted and image-guided photodynamic and chemotherapy with on-demand drug release upon irradiation with a single light source. Angew. Chem. Int. Ed 53, 7163–7168.

102. Yang G-G, Zhang H, Zhang D-Y, Cao Q, Yang J, Ji L-N, and Mao Z-W (2018). Cancer-specific chemotherapeutic strategy based on the vitamin K3 mediated ROS regenerative feedback and visualized drug release in vivo. Biomaterials 185, 73–85. [PubMed: 30227273]

103. Li J, Ke W, Wang L, Huang M, Yin W, Zhang P, Chen Q, and Ge Z (2016). Selfsuffic ing H2O2-responsive nanocarriers through tumor-specific H2O2 production for synergistic oxidation-chemotherapy. J. Control Release 225, 64–74. [PubMed: 26806789]

104. Dai L, Li X, Duan X, Li M, Niu P, Xu H, Cai K, and Yang H (2019). A pH/ROS cascade-responsive charge-reversal nanosystem with self-amplified drug release for synergistic oxidation-chemotherapy. Adv. Sci 6, 1801807.

105. Ye M, Han Y, Tang J, Piao Y, Liu X, Zhou Z, Gao J, Rao J, and Shen Y (2017). A tumor-specific cascade amplification drug release nanoparticle for overcoming multidrug resistance in cancers. Adv. Mater 29, 1702342.

106. Wang S, Yu G, Wang Z, Jacobson O, Tian R, Lin LS, Zhang F, Wang J, and Chen X (2018). Hierarchical tumor microenvironment-responsive nanomedicine for programmed delivery of chemotherapeutics. Adv. Mater 30, 1803926.

107. Zhang F, Zhu G, Jacobson O, Liu Y, Chen K, Yu G, Ni Q, Fan J, Yang Z, Xu F, et al. (2017). Transformative nanomedicine of an amphiphilic camptothecin prodrug for long circulation and high tumor uptake in cancer therapy. ACS Nano 11, 8838–8848. [PubMed: 28858467]

108. Guo X, Wang L, Duval K, Fan J, Zhou S, and Chen Z (2018). Dimeric drug polymeric micelles with acid-active tumor targeting and FRET-traceable drug release. Adv. Mater 30, 1705436.

109. Wang S, Zhang F, Yu G, Wang Z, Jacobson O, Ma Y, Tian R, Deng H, Yang W, Chen Z-Y, et al. (2020). Zwitterionic-tocationic charge conversion polyprodrug nanomedicine for enhanced drug delivery. Theranostics 10, 6629–6637. [PubMed: 32550894]

110. Ke W, Li J, Mohammed F, Wang Y, Tou K, Liu X, Wen P, Kinoh H, Anraku Y, Chen H, et al. (2019). Therapeutic polymersome nanoreactors with tumorspecific activable cascade reactions for cooperative cancer therapy. ACS Nano 13, 2357–2369. [PubMed: 30699292]

111. Ma X, Huang X, Moore Z, Huang G, Kilgore JA, Wang Y, Hammer S, Williams NS, Boothman DA, and Gao J (2015). Esterase-activatable β-lapachone prodrug micelles for nqo1-targeted lung cancer therapy. J. Control Release 200, 201–211. [PubMed: 25542645]

112. Saravanakumar G, Kim J, and Kim WJ (2017). Reactive-oxygen-species-responsive drug delivery systems: promises and challenges. Adv. Sci 4, 1600124.

113. Holohan C, Van Schaeybroeck S, Longley DB, and Johnston PG (2013). Cancer drug resistance: an evolving paradigm. Nat. Rev. Cancer 13, 714–726. [PubMed: 24060863]

Progress and Potential

Low bioavailability and adverse side effects of untargeted chemotherapeutic drugs are the major constraints that limit the efficacy of chemotherapy. Therefore, it is of great significance to develop precise on-demand drug-delivery systems with high selectivity and responsiveness to enhance anticancer therapy. Stimuli-responsive nanomedicines that can be activated by delicately designed cascade reactions have attracted increasing attention to achieve fine control over the activation process of anticancer agents. This review mainly summarizes recent progress made in cascade drug-release modes. We highlight different kinds of intermediate stimuli (heat, hypoxia, and reactive oxygen species) that are employed in controlling drug-release behaviors. We hope that this review can provide promising directions in the design of cascade reactions-driven drug-delivery systems and expand their applications in future tumor-targeted chemotherapy.
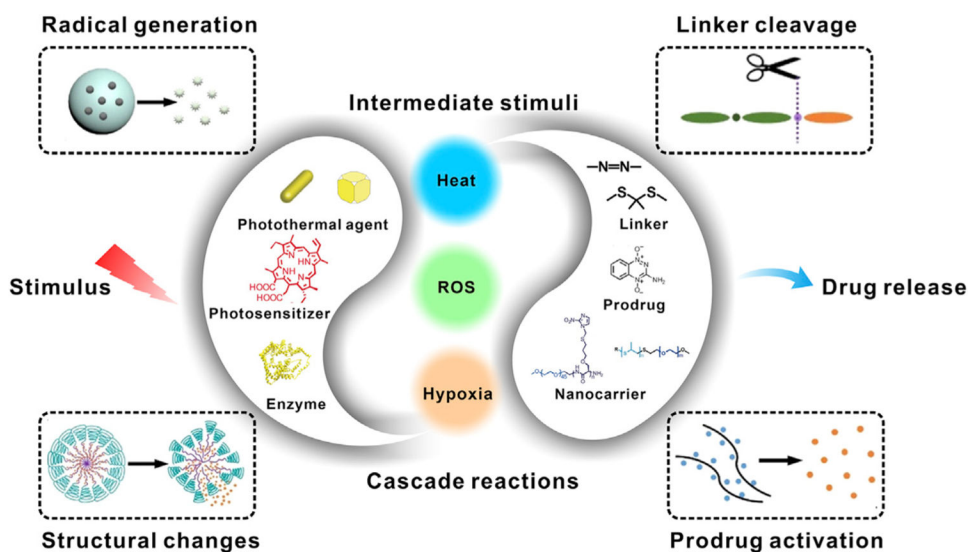
Figure 1. Schematic Illustration of the Cascade Reactions-Driven Drug-Release Strategy in Anticancer Therapy

The nanomedicines are triggered by an internal or external stimulus, generating an intermediate stimulus (e.g., heat, ROS, hypoxia) at tumor site, which can intensify the differences between tumor and normal tissues. The drug-release process will then be further activated by the intermediate stimulus through a certain response, such as radical generation, structural change, linker cleavage, and prodrug activation.
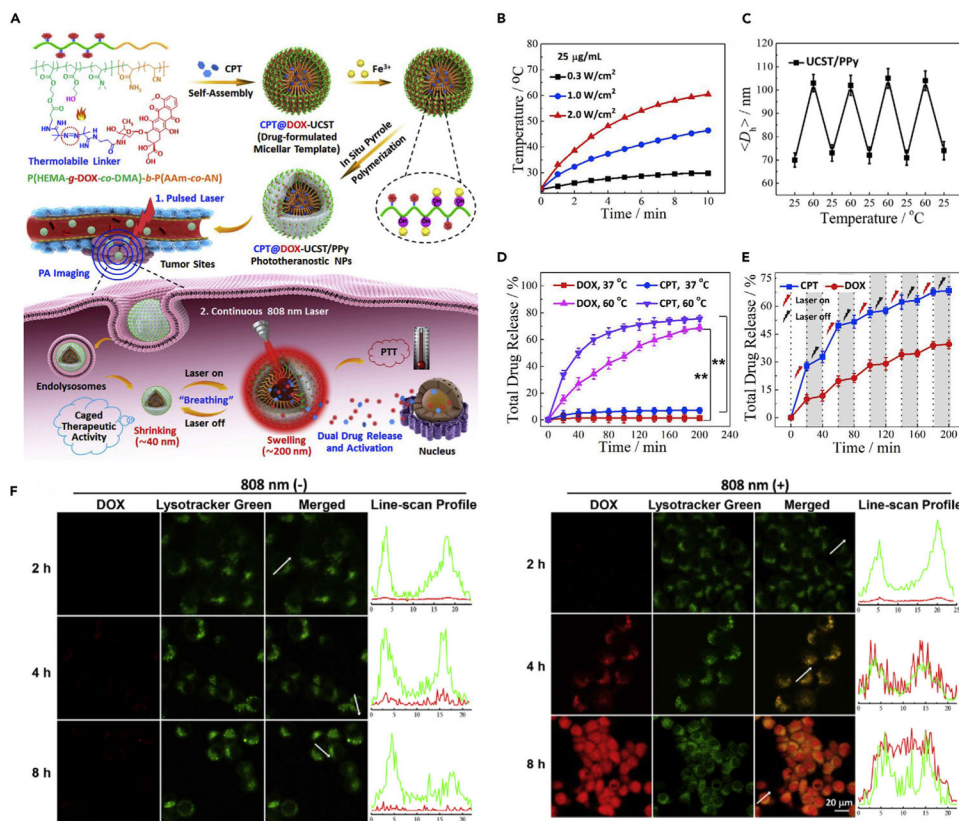
Figure 2. Drug Release Driven by the Cascade of Stimuli-Induced Heating and Heat-Induced Linker Cleavage

(A) Schematic illustration of light-triggered drug-release process.

(B) Temperature elevation profiles of CPT@DOX-UCST/PPy upon laser irradiation.

(C) Size change of UCST/PPy at different temperatures for four cycles.

(D) *In vitro* drug-release behaviors of CPT and DOX from CPT@DOX-UCST/PPy at different temperatures.

(E) *In vitro* drug-release behaviors of CPT and DOX from CPT@DOX-UCST/PPy with periodic laser irradiation (808 nm, 2 W cm^{-2}).

(F) Intracellular drug release of CPT@DOX-UCST/PPy treated without (−) or with (+) light irradiation (808 nm, 2 W cm^{-2}, 5 min).

Reproduced with permission from Yang et al.[30] Copyright 2018, Elsevier.
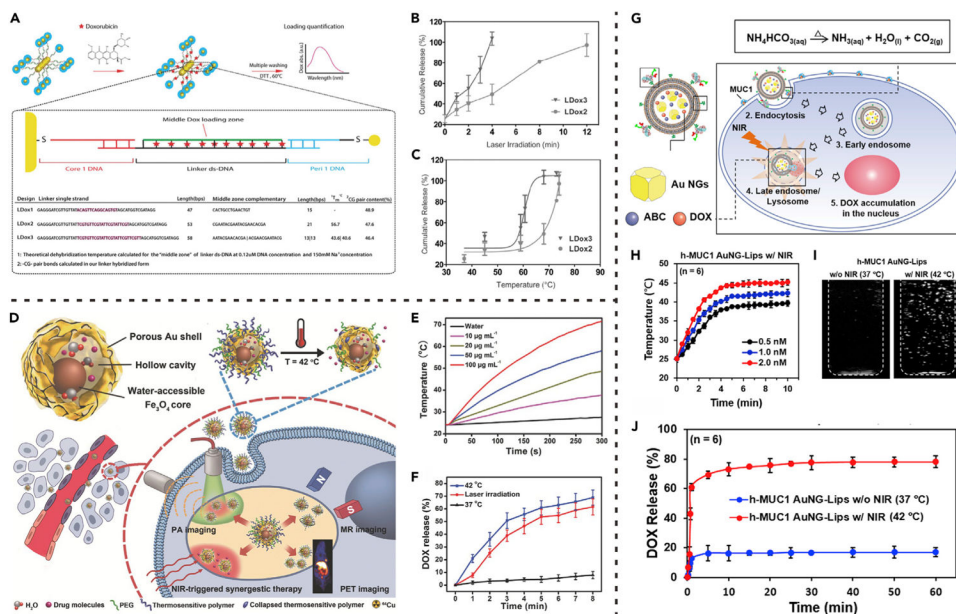
Figure 3. Drug Release Driven by the Cascade of Stimuli-Induced Heating and Heat-Induced Structural Changes of Drug Carriers

(A) GNR core-satellite superstructures prepared by different DNA linker sequences.

(B) Drug release from GNR superstructures triggered by laser irradiation for different time.

(C) Drug release from GNR superstructures triggered by different photothermal temperatures.

(A) to (C) reproduced with permission from Raeesi et al.[32] Copyright 2016, WILEY-VCH Verlag GmbH & Co. KGaA, Weinheim.

(D) Schematic illustration of photothermal heating-triggered drug release from yolk-shell Fe_3O_4@Au NPs.

(E) Photothermal heating curves of the yolk-shell Fe_3O_4@Au NPs under laser irradiation.

(F) Drug release from the yolk-shell Fe_3O_4@Au NPs at different temperatures or under laser irradiation.

(D) to (F) reproduced with permission from Lin et al.[34] Copyright 2017, WILEY-VCH Verlag GmbH & Co. KGaA, Weinheim.

(G) Schematic illustration of nanocarrier (AuNG-Lips) destruction caused by photothermal heating-triggered bubble generation.

(H) Photothermal heating curves of the AuNG-Lips under laser irradiation.

(I) Ultrasound images showing photothermal heating-triggered bubble generation from the AuNG-Lips.

(J) Drug release from the AuNG-Lips at 37°C or 42°C (maintained by laser irradiation). (G) to (J) reproduced with permission from Chuang et al.[35] Copyright 2016, Elsevier.
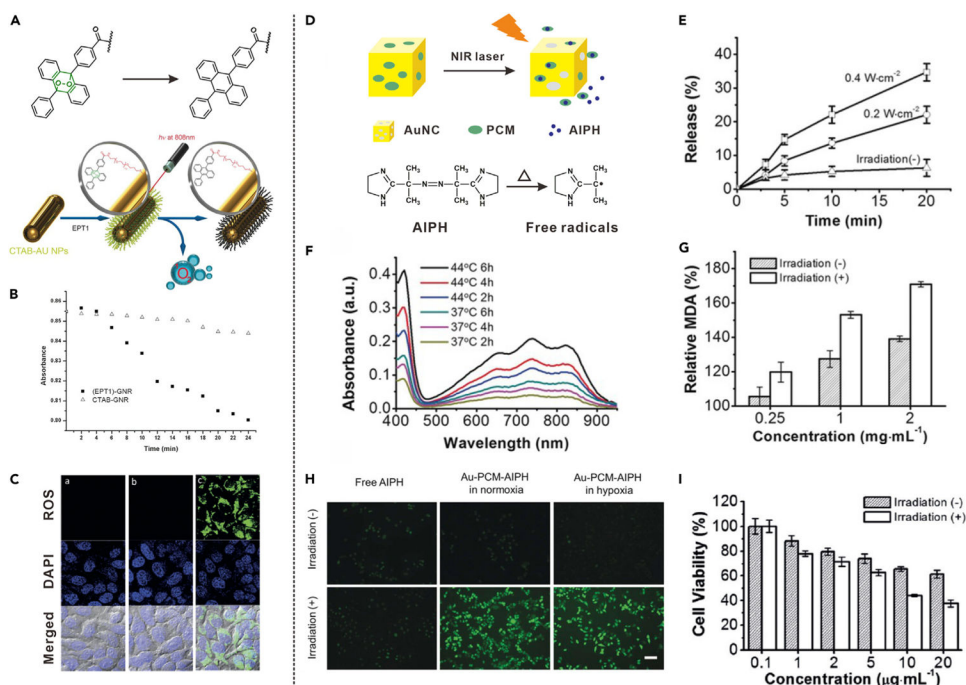
Figure 4. Drug Release Driven by the Cascade of Stimuli-Induced Heating and Heat-Induced Generation of ROS or Free Radicals

(A) Schematic illustration showing NIR light-induced heating and subsequent $^1O_2$ generation from EPT1.

(B) Absorption spectra of DPBF for detection of NIR light-induced $^1O_2$ generation.

(C) CLSM images of cells incubated with ROS sensor and different formulations with laser irradiation. Left: no additive; middle: PEG-AuNR; right: EPT1-AuNR.

(A) to (C) reproduced with permission from Kolemen et al.[36] Copyright 2016, WILEY-VCH Verlag GmbH & Co. KGaA, Weinheim.

(D) Schematic illustration showing NIR light-induced decomposition of AIPH and release of free radicals.

(E) NIR light-triggered AIPH release from Au-PCM-AIPH.

(F) Absorption spectra of ABTS upon incubation with Au-PCM-AIPH at different temperatures.

(G) MDA level changes in RBCs upon incubation with Au-PCM-AIPH.

(H) Intracellular radical generation from Au-PCM-AIPH in different conditions.

(I) Viability of A549 cells treated with Au-PCM-AIPH. (D) to (I) reproduced with permission from Shen et al.[37] Copyright 2017, WILEY-VCH Verlag GmbH & Co. KGaA, Weinheim.
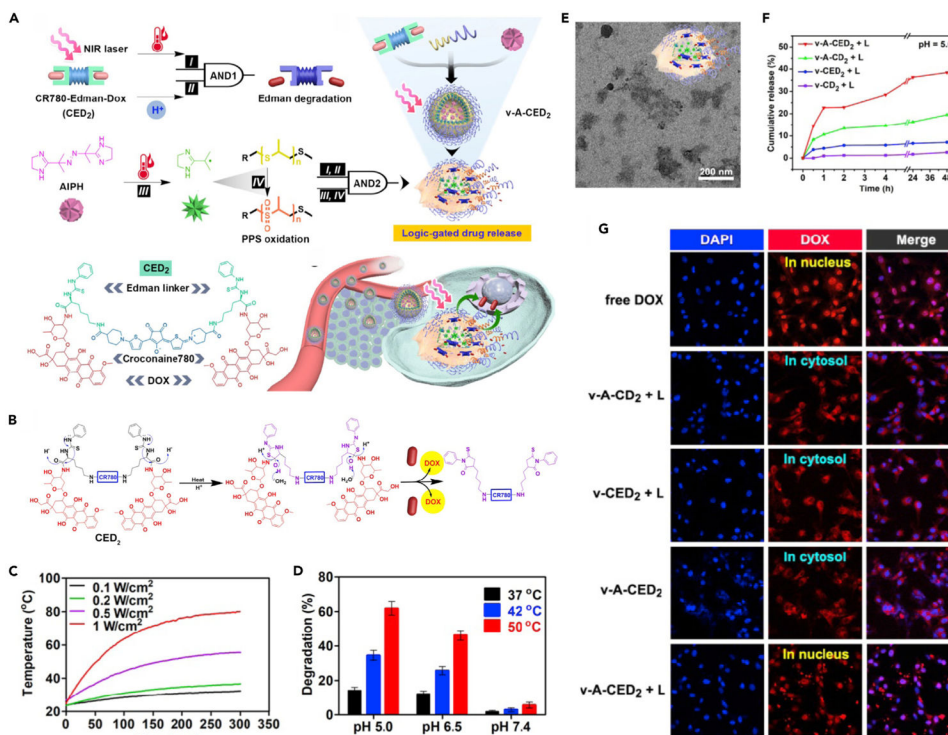
Figure 5. Drug Release Driven by the Cascade of Stimuli-Induced Heating and Heat-Induced Multiple Responses (Linker Cleavage, Radical Generation, and Structural Change)

(A) Schematic illustration of programmable drug release from logic-gated v-A-CED$_2$.

(B) Schematic illustration showing the drug-release mechanism of CED$_2$ based on Edman degradation.

(C) Photothermal heating curves of CED$_2$ under laser irradiation.

(D) Degradation percentage of CED$_2$ at different temperatures and pH values.

(E) TEM image of v-A-CED$_2$ after 30 min of incubation at 50°C.

(F) Light-triggered drug release from different nanovesicles at pH 5.

(G) CLSM images of U87MG cells incubated with different formulations with or without laser irradiation.

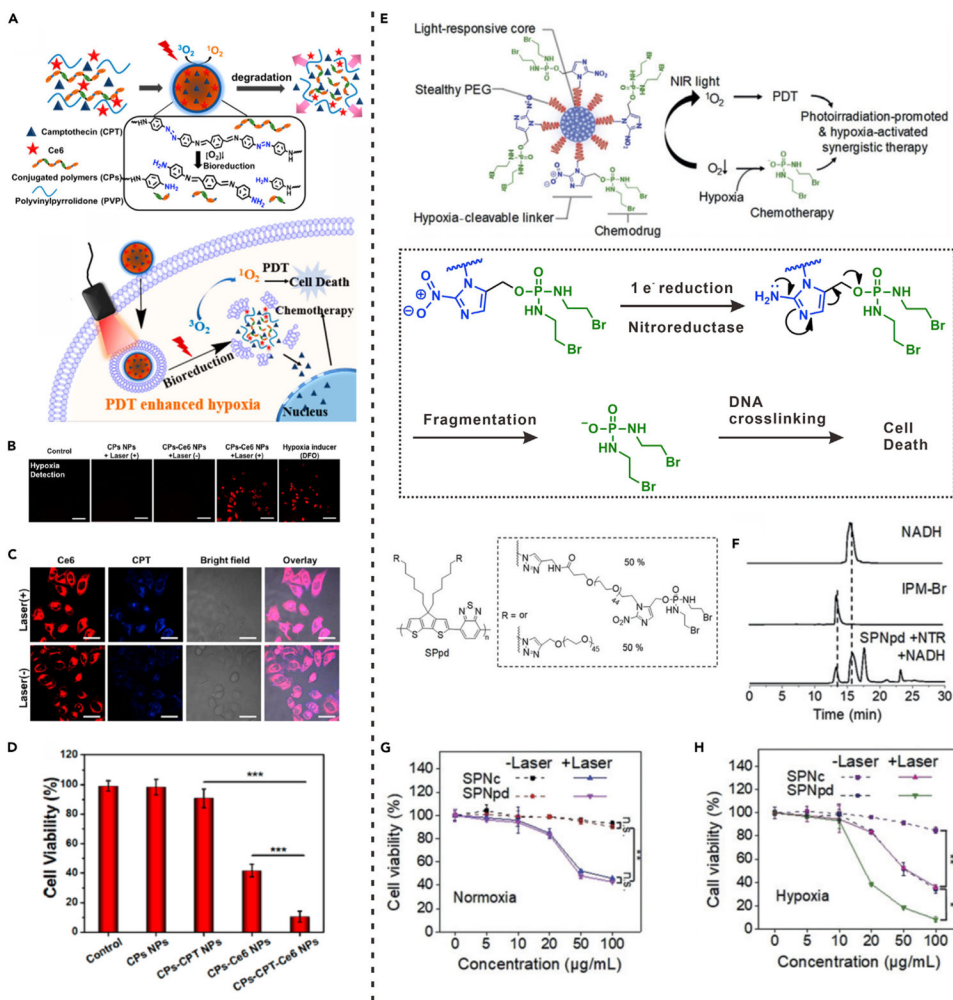Reproduced with permission from Tang et al.[39] Copyright 2019, Ivyspring International Publisher.

Figure 6. Drug Release Driven by the Cascade of Stimuli-Induced Hypoxia and Hypoxia-Induced Linker Cleavage

(A) Schematic illustration of hypoxia-responsive mechanism of CPs-CPT-Ce6 NPs.

(B) Intracellular hypoxia detection of HeLa cells with different treatments.

(C) Fluorescence images of HeLa cells incubated with CPs-CPT-Ce6 NPs.

(F) Viability of HeLa cells with different treatments and laser irradiation. (***p < 0.001).

(A) to (D) reproduced with permission from Zhang et al.[40] Copyright 2018, American Chemical Society.

(E) Schematic illustration showing the hypoxia-activated drug release from SPNpd.

(F) HPLC profiles of free IPM-Br, NADH and SPNpd incubated with NTR and NADH.

(G and H) Viabilities of 4T1 cells incubated with SPNpd and SPNc with or without laser irradiation in normoxic (G) and hypoxic (H) conditions. (E) to (H) reproduced with permission from Cui et al.[41] Copyright 2019, WILEY-VCH Verlag GmbH & Co. KGaA, Weinheim.
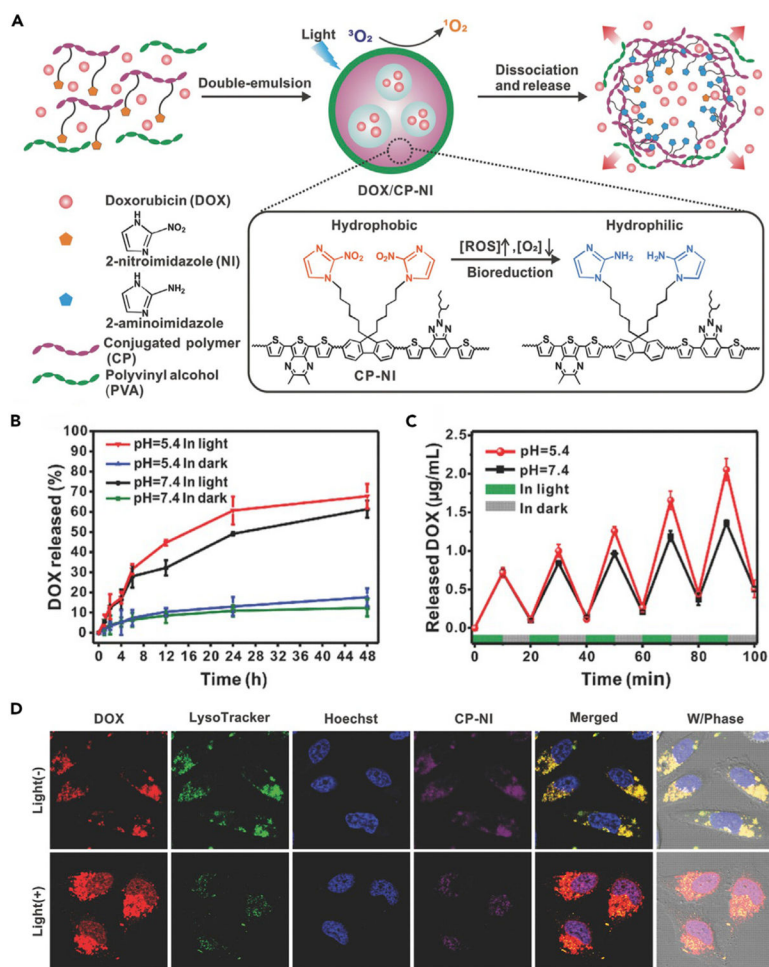
Figure 7. Drug Release Driven by the Cascade of Stimuli-Induced Hypoxia and Hypoxia-Induced Dissociation of Nanocarrier

(A) Schematic illustration showing the application of DOX/CP-NI NPs for drug delivery.

(B) *In vitro* drug release from DOX/CP-NI NPs in different conditions.

(C) Pulsatile release profile of DOX/CP-NI NPs at different pH for light/dark cycles.

(D) CLSM images of HeLa cells treated with different formulations.

Reproduced with permission from Qian et al.[42] Copyright 2016, WILEY-VCH Verlag GmbH & Co. KGaA, Weinheim.
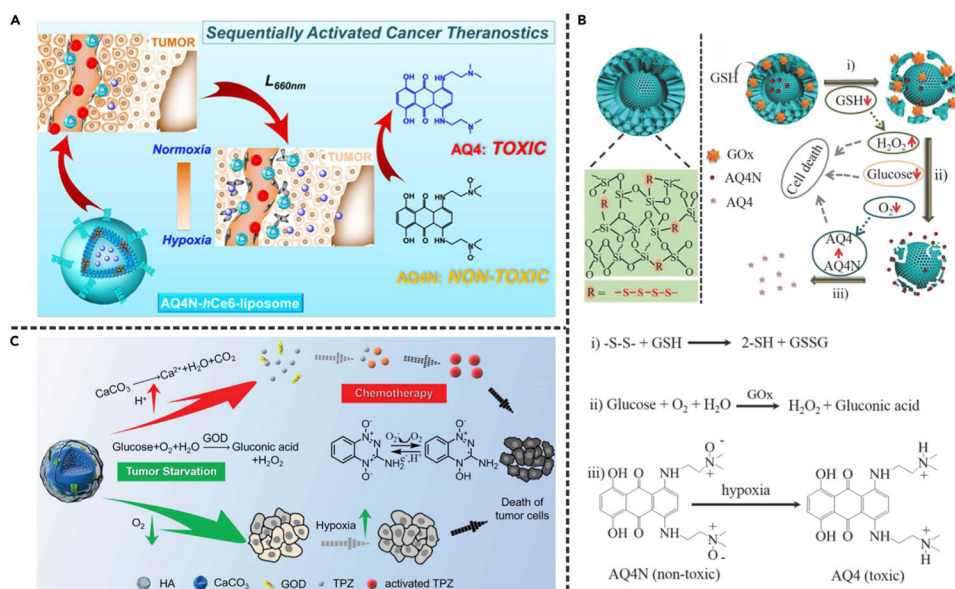
Figure 8. Drug Release Driven by the Cascade of Stimuli-Induced Hypoxia and Hypoxia-Induced Activation of Prodrugs

(A) Schematic illustration showing the application of AQ4N-hCe6-liposome for activation of AQ4N prodrug. Reproduced with permission from Feng et al.[43] Copyright 2016, American Chemical Society.

(B) Schematic illustration showing the application of YS-DMONs for synergistic cancer therapy. (i) Intracellular delivery of GOD and AQ4N caused by GSH-triggered cleavage of tetrasulfide bond; (ii) GOD-mediated catalytic reaction led to oxygen consumption and formation of hypoxic environment; (iii) hypoxia-induced activation of AQ4N prodrug. Reproduced with permission from Yang et al.[44] Copyright 2018, WILEY-VCH Verlag GmbH & Co. KGaA, Weinheim.

(C) Schematic illustration showing the application of AC-TGH for activation of TPZ prodrug. Reproduced with permission from Zhang et al.[45] Copyright 2018, WILEY-VCH Verlag GmbH & Co. KGaA, Weinheim.
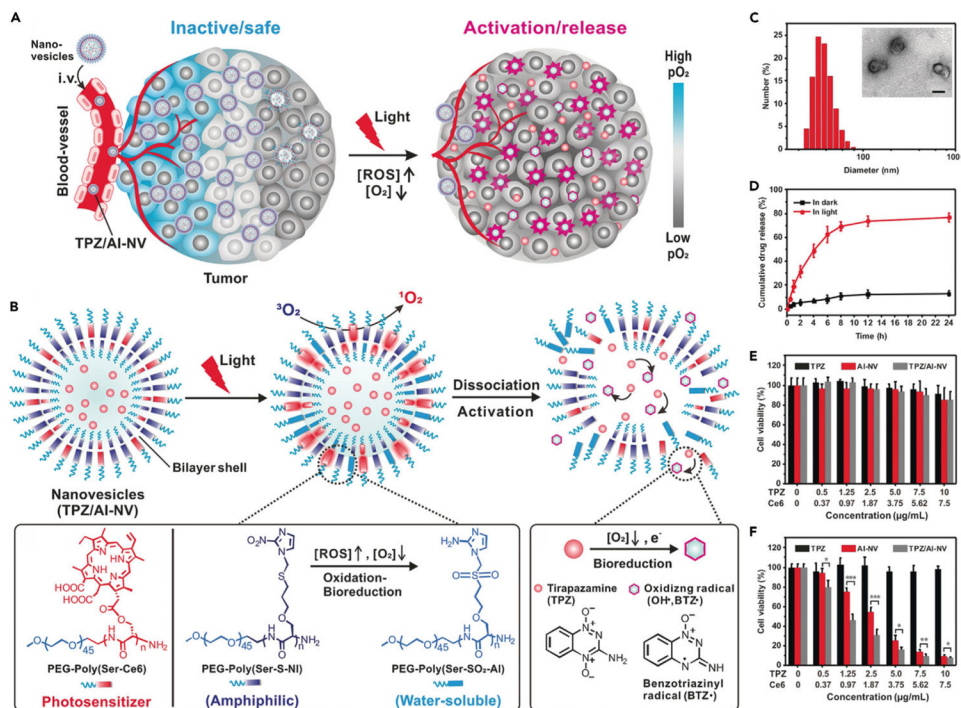
Figure 9. Drug Release Driven by the Cascade of Stimuli-Induced Hypoxia and Hypoxia-Induced Multiple Responses (Hydrophobic-to-Hydrophilic Transition, Prodrug Activation)

(A) Schematic illustration of light-induced local hypoxia in tumor.

(B) Schematic illustration showing the mechanism of hypoxia-triggered release and activation of TPZ.

(C) Size and morphology changes of TPZ/AI-NV upon light irradiation.

(D) *In vitro* drug release from TPZ/AI-NV in different conditions.

(E and F) Viability of HepG2 cells treated with different formulations in darkness (E) and in light (F). Reproduced with permission from Qian et al.[46] Copyright 2017, WILEY-VCH Verlag GmbH & Co. KGaA, Weinheim.
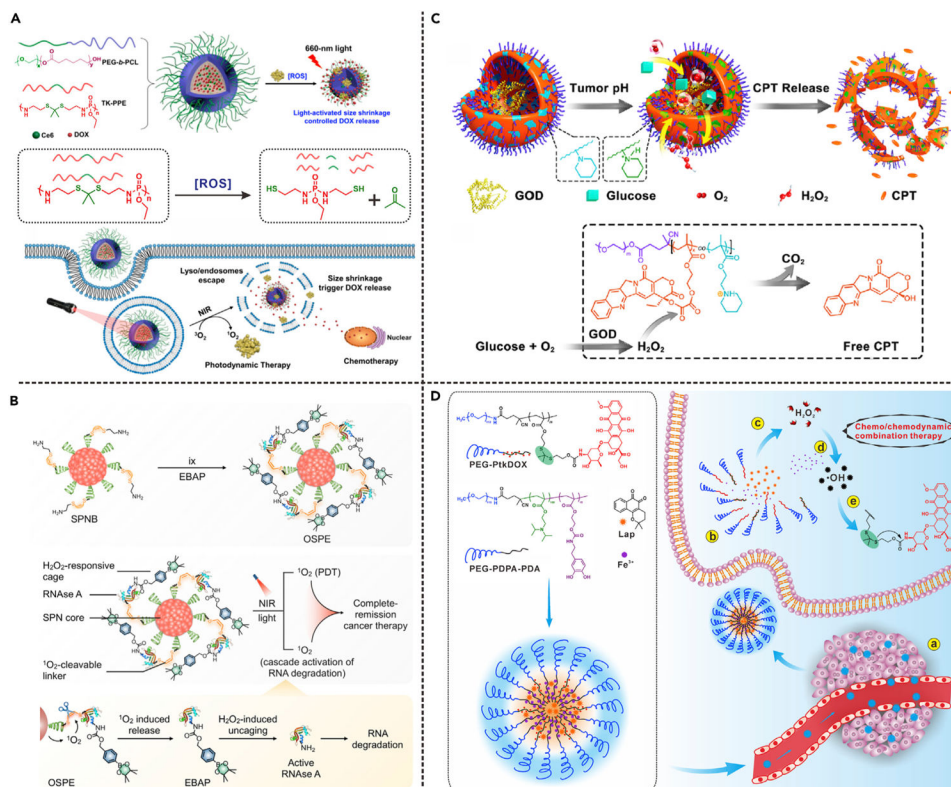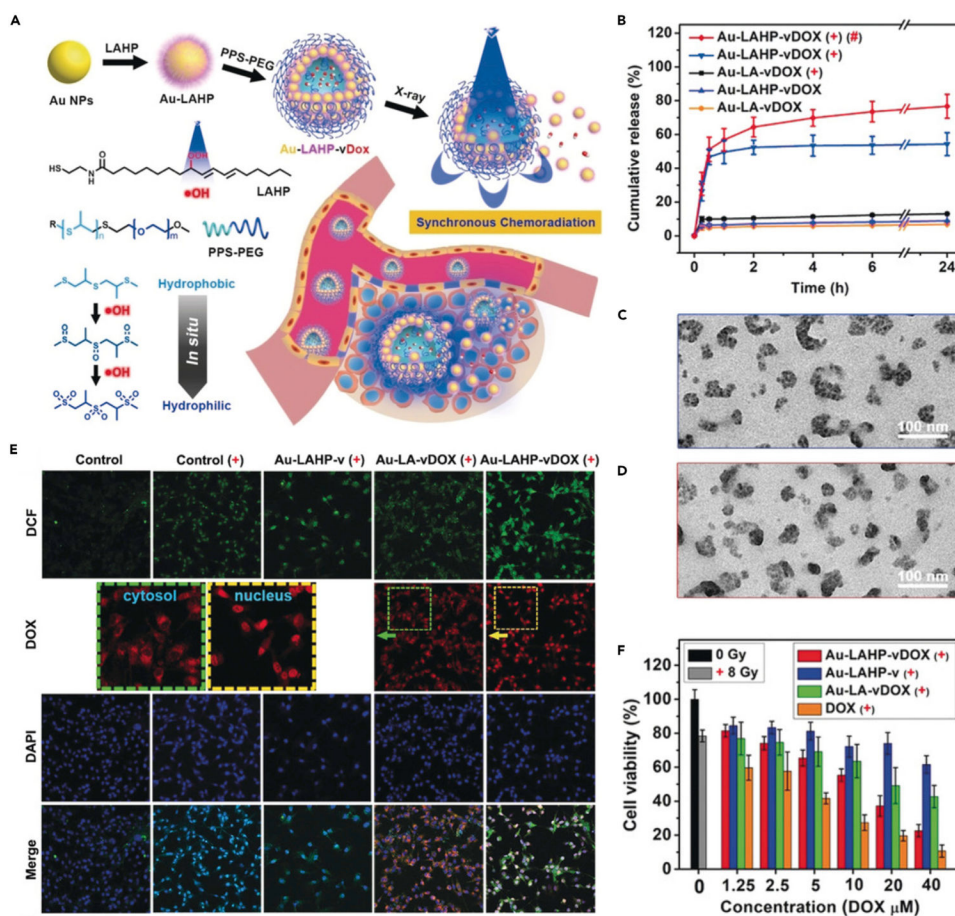
Figure 10. Drug Release Driven by the Cascade of Stimuli-Induced ROS Generation and ROS-Induced Linker Cleavage

(A) $^1O_2$-activated cleavage of TK linker in nanocarrier. Reproduced with permission from Cao et al.[47] Copyright 2017, American Chemical Society.

(B) $^1O_2$-activated cleavage of linker in organic semiconducting pro-nanoenzyme. Reproduced with permission from Li et al.[51] Copyright 2019, American Chemical Society.

(C) H_2O_2-triggered cleavage of peroxalate ester linkage in polyprodrug. Reproduced with permission from Li et al.[52] Copyright 2017, American Chemical Society.

(D) Hydroxyl radical-triggered cleavage of TK linker in polyprodrug. Reproduced with permission from Wang et al.[53] Copyright 2019, WILEY-VCH Verlag GmbH & Co. KGaA, Weinheim.

Figure 11. Drug Release Driven by the Cascade of Stimuli-Induced ROS Generation and ROS-Induced Dissociation of Nanocarrier

+, X-ray irradiation; #, H_2O_2 (100 μM).

(A) Schematic illustration showing X-ray-triggered drug release from the Au-LAHP-vDOX.

(B) *In vitro* drug release from different formulations.

(C and D) TEM images of X-ray-irradiated Au-LAHP-vDOX upon incubation with PBS (C) and H_2O_2 (D).

(E and F) CLSM images (E) and viability (F) of U87MG cells treated with different formulations.

Reproduced with permission from Zhou et al.[54] Copyright 2018, WILEY-VCH Verlag GmbH & Co. KGaA, Weinheim.
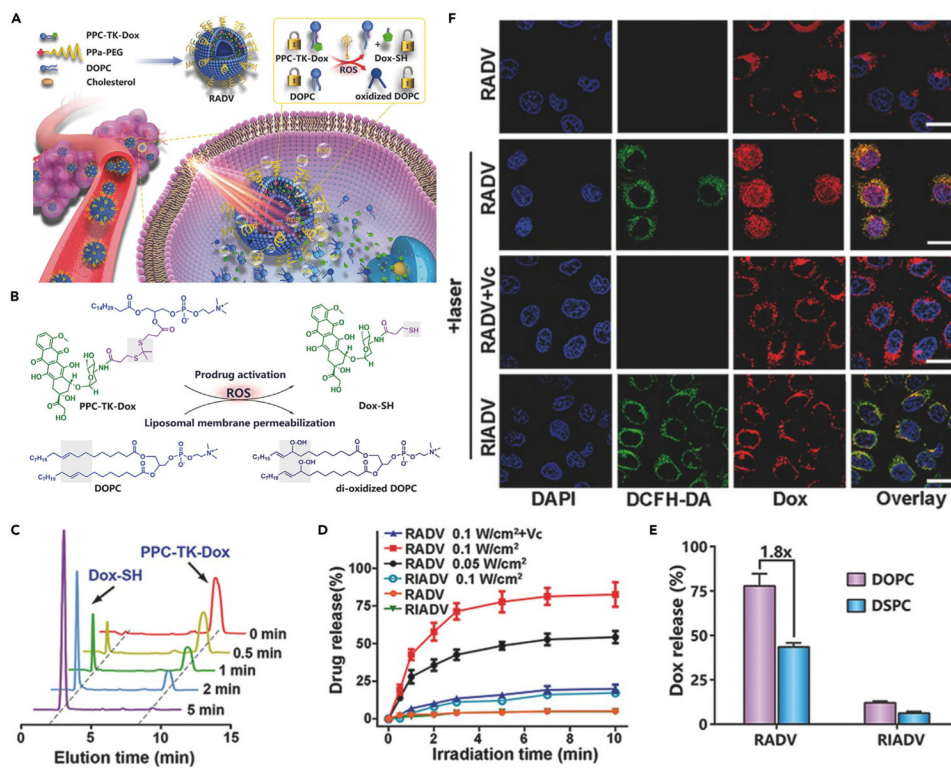
Figure 12. Drug Release Driven by the Cascade of Stimuli-Induced ROS Generation and ROS-Induced Multiple Responses (Structural Change of Nanocarrier and Linker Cleavage)

(A) Schematic illustration showing the working mechanism of RADV.

(B) Chemical structure changes of DOX prodrug and DOPC upon ROS treatment.

(C) HPLC profiles of PPC-TK-DOX with different times of laser irradiation.

(D) *In vitro* drug release from RADV and RIADV with or without light irradiation.

(E) Light-triggered DOX release from vesicles prepared by DOPC or DSPC.

(F) CLSM images of RADV- and RIADV-treated 4T1 cells.

Reproduced with permission from Zhou et al.[55] Copyright 2017, WILEY-VCH Verlag GmbH & Co. KGaA, Weinheim.

Table 1.

Summary of Stimuli-Responsive Materials in Cascade Anticancer Therapy

Stimuli	Responsive Categories	Materials	Triggering Methods	Responsive Groups	Payloads	Therapeutic Applications	Reference
Heat	linker cleavage	CPT@DOX-UCST/PPy	NIR light	thermolabile azo bond	DOX	PTT/chemotherapy	Yang et al. [30]
	structural changes of drug carriers	transfer DNA(DOX)-NRs	NIR light	DNA double helix	DOX	thermo-chemotherapy	Xiao et al. [31]
		LDox1/LDox2/LDox3	NIR light	DNA linkers	DOX	PTT/chemotherapy	Raeesi et al. [32]
		Au nanocages covered by a copolymer	NIR light	pNIPAm-co-AAm	DOX	chemotherapy	Yavuz et al. [33]
		yolk-shell Fe_3O_4@Au NPs	NIR light	pNIPAm-co-AAm	DOX	PTT/chemotherapy	Lin et al. [34]
		AuNG-Lips	NIR light	ammonium bicarbonate (ABC)	DOX	NIR-responsive tumor chemotherapy	Chuang et al. [35]
	radical generation	EPT1-GNR	NIR light	EPT1	EPT1	PDT	Kolemen et al. [36]
		Au-PCM-AIPH	NIR light	AIPH	AIPH	PTT/PDT	Shen et al. [37]
		$CuFeSe_2$-AIPH@BSA	NIR light (I/II)	AIPH	AIPH	imaging-guided and NIR-II-mediated PTT/PDT	Yang et al. [38]
	multiple responses	v-A-CED$_2$	NIR light	Edman linker/AIPH	DOX/AIPH	chemotherapy/PDT	Tang et al. [39]
Hypoxia	linker cleavage	CPs-CPT-Ce6 NP	red light	azo group	CPT	PDT/chemotherapy	Zhang et al. [40]
		SPNpd	NIR light	nitro groups	IPM-Br	PDT/chemotherapy	Cui et al. [41]
	hydrophobic-to-hydrophilic transition	DOX/CP-NI NPs	light (532 nm)	NI	DOX	PDT/chemotherapy	Qian et al. [42]
	activation of prodrug	AQ4N-hCe6-liposome	red light	AQ4N prodrug	activated AQ4	PDT/chemotherapy	Feng et al. [43]
		YS-DMONs	GOx	AQ4N prodrug	activated AQ4	GSH depletion/starvation, oxidative cytotoxicity/chemotherapy	Yang et al. [44]
		AC-TGH NPs	GOx	TPZ prodrug	TPZ	starvation therapy/chemotherapy	Zhang et al. [45]
	multiple responses	TPZ/AI-NV	red light	TPZ/NI	TPZ	PDT/chemotherapy	Qian et al. [46]
ROS	linker cleavage	TK-PPE@NP	red light	thioketal linker	DOX	chemotherapy	Cao et al. [47]
		HA-aPS-aCPT NPs	red light	thioketal linker	CPT	PDT/chemotherapy	Phua et al. [48]
		organic semiconducting pro-nanostimulant	NIR light	thioketal linker	NLG919	phototherapy/immunotherapy	Li et al. [49]
		semiconducting polymer nanoblockader (SPNB)	NIR light	thioketal linker	Puromycin	PDT/inhibition of protein synthesis	Li et al. [50]

Stimuli	Responsive Categories	Materials	Triggering Methods	Responsive Groups	Payloads	Therapeutic Applications	Reference
		organic semiconducting pro-nanoenzyme (OSPE)	NIR light	BSDA linker	ribonuclease A (RNase A)	PDT/ degradation of RNA	Li et al.[51]
		Mem@GOD@ZIF-8@BDOX	GOx	boronic ester linker	DOX	starvation therapy/ chemotherapy	Cheng et al.[10]
		GOD@PCPT-NR	GOx	oxalate bonds	CPT	oxidation therapy/ chemotherapy	Li et al.[52]
		PEG-PtkDOX	lap	thioketal linker	DOX	CDT/ chemotherapy	Wang et al. [53]
	hydrophobic-to-hydrophilic transition	Au-LAHP-vDOX	X-ray	sulfide groups	DOX	radiotherapy/ chemotherapy	Zhou et al. [54]
	multiple responses	RADV	red light	unsaturated DOPC/ thioketal linker	DOX	PDT/ chemotherapy	Zhou et al. [55]